Reconfigurable Intelligent Surface Assisted Unified NOMA Framework

Zhihao Han, Xinwei Yue, *Member, IEEE*, Bin Dai, *Member, IEEE*, Rongke Liu, *Senior Member, IEEE* and Arumugam Nallanathan, *Fellow, IEEE*

***Abstract*—This paper investigates the application of reconfigurable intelligent surface (RIS) to assist a unified non-orthogonal multiple access (RIS-U-NOMA) framework. More specifically, the proposed RIS-U-NOMA can be applied to RIS assisted code-domain NOMA (RIS-CD-NOMA) and power-domain NOMA (RIS-PD-NOMA). To characterize the performance of RIS-U-NOMA framework, we derive new approximated expressions of outage probability and ergodic rate for a pair of users. Based on the asymptotic expressions, the diversity orders and high signal-to-noise ratio (SNR) slopes for the nearby and distant users are obtained in details. In addition, the system throughput of RIS-U-NOMA is discussed in the delay-limited and delay-tolerant transmission modes. Monte Carlo simulations are provided to verify the analytical results and indicate that: 1) The outage behaviors of RIS-U-NOMA are better than that of RIS assisted orthogonal multiple access (RIS-OMA) and conventional full/half-duplex decode-and-forward relays; 2) The RIS-U-NOMA networks are competent to obtain superior performance in ergodic rate and achieve steeper slope than RIS-OMA; and 3) The delay-limited and delay-tolerant throughput of RIS-CD-NOMA outperform that of RIS-PD-NOMA.**

***Index terms*—** Non-orthogonal multiple access, reconfigurable intelligent surface, a unified framework, outage probability, ergodic rate

I. Introduction

As the front-edge technology to promote the next generation of wireless communication systems, the sixth generation (6G) communication networks will realize the intelligent connection of everything and promote the popularization of telemedicine, autonomous driving, virtual reality, and other applications. To enable these, the 6G networks ought to meet more stringent requirements in metrics, such as higher peak rates, greater connection density, and enhanced spectrum/energy efficiency [1]. Non-orthogonal multiple access (NOMA) has the ability to serve multiple users in one physical resource element (RE) and significantly support massive connections of networks, which has been considered to be one of the key technologies in 6G networks [2–4]. Applying the successive interference cancellation (SIC) at the receivers, NOMA is capable of achieving the boundary of the capacity region [5]. In addition, NOMA strikes a good compromise between system throughput and user fairness, which is a great improvement over traditional opportunistic communication [6]. However, a large number of NOMA schemes have been proposed in the past decade, but no unified standard has been formed.

Hence, the unified framework of NOMA has attracted extensive attention of scholars. The authors of [7] evaluated a unified NOMA framework by analyzing its outage behaviors over Rayleigh fading channel, where the power-domain NOMA (PD-NOMA) was discussed as a special case. As mentioned in [8], the resource allocation and user association schemes have been investigated for the unified NOMA enabled heterogeneous ultra-dense networks. More generally, NOMA has been divided into PD-NOMA and code-domain NOMA (CD-NOMA) [9, 10]. The authors in [11] identified that the outage probability of PD-NOMA mainly depends on the target rate and power allocation. It was shown that reasonable power allocation leads to enhanced ergodic rate performance. By integrating the concept of PD-NOMA to candidate technologies of B5G networks, different rate scenarios have been proposed [12]. To reduce transmission delay, PD-NOMA was incorporated grant-free to strengthen the overall packet loss behavior [13]. Regarding CD-NOMA, the bit error rate (BER) performance has been characterized in sparse code multiple access (SCMA) system with designed codebooks [14]. Based on the joint design of transmitter and receiver, the authors in [15] proposed a non-orthogonal pattern division multiple access scheme. As propounded in [16], the authors analyzed a relay-based pattern division multiple access and derived outage probability to evaluate the system performance. Driven by this trend, the authors of [17] introduced a pattern design scheme based on the superposition of orthogonal-building blocks, which achieves considerable performance gains compared to traditional pattern division random access. Furthermore, the evolution from NOMA to next generation multiple access (NGMA) was explored in [18]. The authors of [19] highlighted several practical challenges and applications of NGMA, which brought a new direction to the NOMA scheme in the 6G era.

Recently, the emergence of reconfigurable intelligent surface (RIS) has attracted widespread attention in the academic community [20–22]. The working principle of RIS was described in [23], where metasurfaces and reflectarrays were discussed

Z. Han is with the School of Electronic and Information Engineering, Beihang University, Beijing 100191, China (email: hzh_95@buaa.edu.cn).

X. Yue is with the Key Laboratory of Modern Measurement & Control Technology, Ministry of Education and also with the School of Information and Communication Engineering, Beijing Information Science and Technology University, Beijing 100101, China (email: xinwei.yue@bistu.edu.cn).

B. Dai is with the School of Internet of Things, Nanjing University of Posts and Telecommunications, Nanjing, 210003, China (e-mail: daibin@njupt.edu.cn).

R. Liu is with the School of Electronic and Information Engineering, Beihang University, Beijing 100191, China, and also with Shenzhen Institution of Beihang University, Shenzhen 518000, China (email: rongke_liu@buaa.edu.cn).

A. Nallanathan is with the School of Electronic Engineering and Computer Science, Queen Mary University of London, London E1 4NS, U.K. (email: a.nallanathan@qmul.ac.uk)

as two implementations. The authors of [24] designed the phase shifts of RIS elements and power allocation of the base station, obtaining higher energy efficiency in comparison with conventional amplify-and-forward relays. According to the characteristic of RIS assisted MISO downlink system, the authors jointly designed beamforming and phase vectors of RIS to maximize the weighted sum rate, where the imperfect/perfect channel state information were taken into consideration [25]. To provide valuable insights into the physical-layer security, the authors in [26] formulated an alternating optimization algorithm to maximize the secrecy rate of RIS assisted multi-antenna systems.

Additionally, the application of RIS in NOMA has become a research hotspot [27–30], which can be considered a win-win application. In order to shed light on this issue, the authors of [31] derived the BER expression in a RIS assisted downlink PD-NOMA (RIS-PD-NOMA) system, which has a better reliability than conventional NOMA systems according to the simulation result. From the perspectives of a simple transmission design for RIS-PD-NOMA networks, the authors in [32] observed the theoretical and simulation results for its outage performance. Inspired by this point, a low-complexity phase selection method was raised [33]. The authors researched the performance of RIS-PD-NOMA in random discrete phase shifting and coherent phase shifting. Moreover, it is obvious that passive beamforming weights improve the performance of outage probability, ergodic rate and spectral/energy efficiency by machine learning in RIS-PD-NOMA [34]. Concerning CD-NOMA integrated with RIS (RIS-CD-NOMA), the symbol error rate of RIS assisted SCMA systems was analyzed in [35], where the effects of reflecting elements number and phase shifts were considered. To improve the performance of BER, the authors of [36] employed a modified decoding scheme, which can also reduce the decoding complexity of the message passing algorithm for RIS-CD-NOMA. What's more, RIS assisted rate-splitting multiple access has been investigated in [37], where the outage behavior of cell-edge users is explored to demonstrate its performance advantages over conventional RIS-NOMA.

A. Motivation and Contributions

The aforementioned research works have provided a solid foundation for understanding the performance of RIS-PD-NOMA and RIS-CD-NOMA networks, but a unified framework for RIS assisted NOMA networks has not been well studied. The authors of [38] evaluated the outage probability and energy efficiency with the imperfect/perfect SIC (ipSIC/pSIC) for a practical RIS-NOMA transmission design. However, only the case of PD-NOMA has been considered, which will lead to a poor outage performance in the high-date rate scenario. Based on a unified transceiver design framework, the authors in [39] proposed an overview of NOMA transmission scheme, while the RIS was out of consideration. In practical applications, the fixed NOMA scheme may not always meet the system demands, and also limits the effectiveness and flexibility of NOMA. According to various scenarios, adopting different NOMA schemes becomes the trend in the future. A unified framework can flexibly adjust the system parameters and select the appropriate NOMA mode for users according to the scenarios and existing system resources. This can provide a performance reference for the intelligent allocation of resources in the intelligent radio environment. In addition, the impact of RIS on various NOMA schemes also needs to be carefully evaluated. To the best of our knowledge, there is no related work analyzing the performance of RIS assisted unified NOMA (RIS-U-NOMA) framework, which prompts us to develop this paper. More specifically, we investigate the performance of a pair of users, i.e., the nearby user n and distant user m, in RIS-U-NOMA networks in terms of the outage probability, the ergodic rate and the system throughput. According to the above description, the main contributions of our paper are summarized as follows:

1) We derive the approximated and asymptotic expression of the outage probability for user n with ipSIC/pSIC and user m for RIS-U-NOMA. Based on the asymptotic expressions in high signal-to-noise ratio (SNR) regime, we obtain the corresponding diversity orders. Due to the influence of residual interference, the outage probability for user n with ipSIC tends to the error floor in high SNR region and achieves $zero$ diversity order. Furthermore, we discuss the outage behaviors of RIS-PD-NOMA as the special case of RIS-U-NOMA ($Q = 1$).
2) We compare the outage probability of RIS-U-NOMA, RIS-OMA and conventional full/half-duplex decode-and-forward (FD/HD-DF) relays. It is demonstrated that the outage behaviors of RIS-U-NOMA with pSIC are better than that of RIS-OMA and conventional relays. With the Rician factor κ, the number of subcarriers Q and the reconfigurable elements K increase, the RIS-U-NOMA network can achieve higher outage performance.
3) We derive the approximated expressions and corresponding upper bounds of the ergodic rate for a pair of users in the RIS-U-NOMA networks. Their high SNR slopes are characterized as a performance indicator of ergodic rate. It is observed that the throughput ceiling will be met for user m at high SNRs. With the reduction of subcarriers and reconfigurable elements, the ergodic rate of RIS-U-NOMA networks becomes smaller. We identify that the ergodic rate of RIS-U-NOMA is better than that of RIS-OMA.
4) We appraise the system throughput performance of the RIS-U-NOMA networks in delay-limited and delay-tolerant modes. The system throughput for RIS-CD/PD-NOMA with pSIC is better than that with ipSIC. Meanwhile, the system throughput with pSIC will converge to the same constant R_s in high SNR region. When the residual interference is small, the throughput performance of ipSIC is very close to that of pSIC. With the value of residual interference increasing, the system throughput with ipSIC will significantly decrease and tend to the single-user rate.

B. Organization and Notations

The remainder of this paper is organized as follows. In Section II, we present the system model of the RIS-U-NOMA

framework. The outage probability and diversity order of RIS-U-NOMA are obtained in Section III. Exactly speaking, the approximated and asymptotic expressions of outage probability are derived. The ergodic rate and system throughput are analysed in Section IV. Section V presents the numerical results and verifies the outcome of the theoretical research. Finally, Section VI concludes the paper. The proofs of mathematics are provided in the Appendix.

The main notations used in this paper will be given in the following. The probability density function (PDF) and cumulative distribution function (CDF) of a random variable Z are expressed as $f_Z(\cdot)$ and $F_Z(\cdot)$, respectively; The expectation and variance operations are given by $\mathbb{E}\{\cdot\}$ and $\mathbb{D}\{\cdot\}$, respectively; $\|\cdot\|^2$ represents Euclidean two norm of a vector; $\mathbf{I}_Q$ is a $Q \times Q$ identity matrix; $diag(\cdot)$ denotes a diagonal matrix; The conjugate-transpose operation is represented by $(\cdot)^H$.

II. System Model

Consider a RIS assisted unified downlink NOMA transmission scenarios as shown in Fig. 1, where the superposed signals in multiple subcarriers or REs are transmitted and then reflected by RIS to M users. More specifically, on the side of base station (BS), one sparse spreading matrix $\mathbf{G}_{Q\times M}$ (i.e, sparse matrix or codebook) is utilized to map the data streams of multiple users into Q subcarriers or REs, in which there are several zero elements within each column and satisfies the relationship $M > Q$. The BS and non-orthogonal users are equipped with single antenna, and the RIS consists of K configurable elements. Owing to the serious blockage, we assume that the line of sight (LoS) components of links from the BS to users are not available, while the non line of sight (NLoS) components are existed. Hence the direct links between the BS and users are modeled as the Rayleigh fading. Since the RIS is usually deployed in places with abundant LoS components, the wireless links from BS to RIS, and then to users are assumed to be Rician fading. To facilitate analysis, we considered that M users are assigned to $M/2$ orthogonal pairs[1]. A pair of users are selected to carry out the NOMA protocol, where the nearby user n and distant user m can be distinguished based on their channel conditions. It is noteworthy that our proposed RIS-U-NOMA framework is valid for both near-field and far-field RIS [40]. For the sake of simplicity, the case where both of the BS and users are in the far-field of the RIS is discussed. The complex channel coefficients from BS to non-orthogonal users, BS to RIS, and then to users are denoted by $\mathbf{h}_\mu$, $\widetilde{\mathbf{h}}_{br} \in \mathbb{C}^{K\times 1}$ and $\widetilde{\mathbf{h}}_{R\mu} \in \mathbb{C}^{K\times Q}$ with $\mu \in \{m, n\}$, respectively. The effective cascade channels from the BS to RIS, and then to user μ are donated as $\widetilde{\mathbf{h}}_{R\mu}^H \mathbf{\Theta}_\mu \widetilde{\mathbf{h}}_{br}$, where $\mathbf{\Theta}_\mu = \text{diag}(\sqrt{\beta_1^\mu} e^{j\theta_1^\mu}, ..., \sqrt{\beta_k^\mu} e^{j\theta_k^\mu}, ..., \sqrt{\beta_K^\mu} e^{j\theta_K^\mu})$ denotes the reflecting phase shifting matrixes of the RIS. $\sqrt{\beta_k^\mu} \in [0, 1]$ and $\theta_k^\mu \in [0, 2\pi)$ denote the energy coefficient and phase shift of the k-th element for reflecting responses, respectively.

[1]Considering a compelling compromise between a pair of users has been identified as an effective way to analyze the performance of NOMA, which is applied in many existing NOMA contributions. It is worth noting that in the RIS-U-NOMA networks, pairing scenarios involving multiple users can further enrich the content, which will be shelved in our future work.

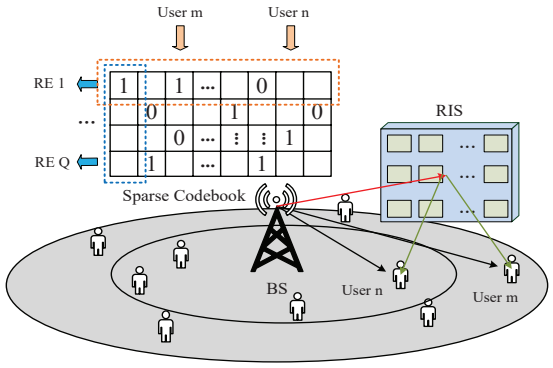

Fig. 1: System model of RIS assisted unified downlink NOMA framework.

Adjusting amplitude of RIS elements can optimize the characteristics of cascade channels, but this is not the focus of this paper. For the sake of simplicity, we consider RIS elements own the same amplitude, i.e., $\beta_1^\mu = \cdots = \beta_K^\mu = 1$.

A. Signal Model

According to the principle of superposition coding [5], the BS broadcasts the superposed signals in multiple subcarriers to active users, where the data streams of each user is spread over one column of sparse matrix. In addition to receiving the signal directly transmitted by the BS, the users also receive the signals reflected by the RIS, and the corresponding signals received can be written as

$$\tilde{\mathbf{y}}_\mu = diag(\mathbf{H}_\mu)(\mathbf{g}_n\sqrt{P_s a_n}x_n + \mathbf{g}_m\sqrt{P_s a_m}x_m) + \mathbf{n}_\mu, \quad (1)$$

where $\mathbf{H}_\mu = \mathbf{h}_\mu + \tilde{\mathbf{h}}_{R\mu}^H \mathbf{\Theta}_\mu \tilde{\mathbf{h}}_{br}$. $x_\mu, \mu \in \{m, n\}$, denotes the unity power signal for user μ, i.e., $\mathbb{E}\{x_\mu^2\} = 1$. Let P_s denote the transmission power at the BS and a_μ is the power allocation factor of user μ, which is considered fixed in our model. The optimal power allocation [41, 42] are ability to improve the performance of NOMA networks, but it is beyond the scope of this paper. $\mathbf{g}_\mu = [g_{\mu 1}, g_{\mu 2}, \cdots, g_{\mu Q}]^T$ is μ-th column of sparse spreading matrix $\mathbf{G}_{Q\times M}$, which represents the mapping relationship of signals to different subcarriers. More specifically, $g_{\mu q} = 1$ and $g_{\mu q} = 0$ means whether the signal of μ-th user is mapped into the q-th subcarrier or not. We assumed that $\mathbf{g}_m$ and $\mathbf{g}_n$ have the same column weights, i.e., $\|\mathbf{g}_m\| = \|\mathbf{g}_n\|$. The design of sparse codebook is able to improve the performance of RIS-U-NOMA, but it is not the focus of this treatise. $\mathbf{n}_\mu \sim \mathcal{CN}(0, N_0\mathbf{I}_Q)$ denotes the additive white Gaussian noise (AWGN). $\mathbf{h}_\mu = [\tilde{h}_{\mu 1}, \tilde{h}_{\mu 2}, \cdots, \tilde{h}_{\mu Q}]^T$ denotes the channel vector from the BS to μ-th user occupying Q subcarriers and $\tilde{h}_{\mu q} = \frac{\sqrt{\eta} h_{\mu q}}{\sqrt{d_\mu^\alpha}}$, where $h_{\mu q} \sim \mathcal{CN}(0, 1)$ is Rayleigh fading channel gain for user μ in the q-th subcarrier. Additionally, d_μ, α and η are the distance from BS to μ-th user, the path loss exponent and the frequency dependent

factor, respectively. Denoting $\tilde{\mathbf{h}}_{br} = [\tilde{h}_{br1}, \tilde{h}_{br2}, \cdots, \tilde{h}_{brQ}]^T$ and $\tilde{\mathbf{h}}_{R\mu}$ can be written as

$$\tilde{\mathbf{h}}_{R\mu} = \begin{pmatrix} \tilde{h}_{R\mu 11} & \tilde{h}_{R\mu 21} & \cdots & \tilde{h}_{R\mu Q1} \\ \tilde{h}_{R\mu 12} & \tilde{h}_{R\mu 22} & \cdots & \tilde{h}_{R\mu Q2} \\ \vdots & \vdots & \ddots & \vdots \\ \tilde{h}_{R\mu 1K} & \tilde{h}_{R\mu 2K} & \cdots & \tilde{h}_{R\mu QK} \end{pmatrix}. \quad (2)$$

Let $\tilde{h}_{brq} = \sqrt{\eta d_{br}^{-\alpha}} \left(\sqrt{\frac{\kappa_1}{\kappa_1+1}} + \sqrt{\frac{1}{\kappa_1+1}} h_{brq} \right)$ and $\tilde{h}_{R\mu qk} = \sqrt{\eta d_{R\mu}^{-\alpha}} \left(\sqrt{\frac{\kappa_2}{\kappa_2+1}} + \sqrt{\frac{1}{\kappa_2+1}} h_{R\mu qk} \right)$, which are the channel coefficients from BS to RIS in q-th subcarrier and the RIS to user μ in k-th reflecting elements, respectively. κ_1 and κ_2 are the Rician factors for above channel coefficients, respectively. Without loss of generality, we consider $\kappa_1 = \kappa_2 = \kappa$ in our paper[2]. The fading gains h_{brq} and $h_{R\mu qk}$ are complex distributed with zero mean and unit variance, i.e., $h_{brq} \sim \mathcal{CN}(0,1)$ and $h_{R\mu qk} \sim \mathcal{CN}(0,1)$.

On the basis of the number of subcarriers, RIS-U-NOMA can be reduced into RIS-CD-NOMA ($Q \neq 1$) and RIS-PD-NOMA ($Q = 1$), respectively. Without loss of generality, we focus on paired users in the following. To enhance the received SNRs and diversity orders, the maximal ratio combiner (MRC) [5] is applied at the μ-th user over Q subcarriers. Note that using MRC is not optimal but with low computational complexity and practicality. Let $\mathbf{w}_\mu = \frac{(diag(\mathbf{H}_\mu)\mathbf{g}_\mu)^*}{\|diag(\mathbf{H}_\mu)\mathbf{g}_\mu\|}$, and then the received signal at the μ-th user can be given by

$$\tilde{y}_\mu = \mathbf{w}_\mu diag\left(\mathbf{H}_\mu\right)\left(\mathbf{g}_n\sqrt{P_s a_n}x_n + \mathbf{g}_m\sqrt{P_s a_m}x_m\right) + \mathbf{w}_\mu \mathbf{n}_\mu. \quad (3)$$

On the principle of SIC, the nearby user n first detects the signal x_m, then subtracts it and decodes its own signal. Hence, the signal-plus-interference-to-noise (SINR) at user n to detect the signal x_m is given by

$$\gamma_{n\to m} = \frac{\rho\left\|diag(\mathbf{h}_n + \tilde{\mathbf{h}}_{Rn}^H \mathbf{\Theta}_n \tilde{\mathbf{h}}_{br})\mathbf{g}_m\right\|^2 a_m}{\rho\left\|diag(\mathbf{h}_n + \tilde{\mathbf{h}}_{Rn}^H \mathbf{\Theta}_n \tilde{\mathbf{h}}_{br})\mathbf{g}_n\right\|^2 a_n + 1}, \quad (4)$$

where $\rho = \frac{P_s}{N_0}$ denotes the transmit SNR.

Based on the operations regarding pSIC and ipSIC, we subtract the decoded signal x_m. Then the SINR of user n to decode the information of itself for pSIC and ipSIC is given by

$$\gamma_n = \frac{\rho\left\|diag(\mathbf{h}_n + \tilde{\mathbf{h}}_{Rn}^H \mathbf{\Theta}_n \tilde{\mathbf{h}}_{br})\mathbf{g}_n\right\|^2 a_n}{\psi\rho\|\mathbf{h_I}\|^2 + 1}. \quad (5)$$

$\psi = 0$ and $\psi = 1$ denote the case of pSIC and ipSIC, respectively. More specifically, $\mathbf{h_I} = [h_{I1}, h_{I2}, \cdots, h_{IQ}]^T$ denotes the residual interference caused by ipSIC on the Q subcarriers, in which $h_{Iq} \sim \mathcal{CN}(0, \Omega_I)$.

[2]By setting different rician factors of the two channel coefficients, we can evaluate the system performance more comprehensively, but this is not the focus of our paper.

The SINR of user m to decode its information by treating the signal of user n as interference is written as

$$\gamma_m = \frac{\rho\left\|diag(\mathbf{h}_m + \tilde{\mathbf{h}}_{Rm}^H \mathbf{\Theta}_m \tilde{\mathbf{h}}_{br})\mathbf{g}_m\right\|^2 a_m}{\rho\left\|diag(\mathbf{h}_m + \tilde{\mathbf{h}}_{Rm}^H \mathbf{\Theta}_m \tilde{\mathbf{h}}_{br})\mathbf{g}_n\right\|^2 a_n + 1}. \quad (6)$$

B. RIS-OMA

In this subsection, the RIS-OMA is selected as one of the baseline for the purpose of comparison, where the RIS is deployed to assist the BS to send the information to user o. The subscript o indicates the orthogonal user. Under the above system conditions, the detecting SNR of user o for RIS-OMA can be given by

$$\gamma_o^{OMA} = \rho\left\|diag(\mathbf{h}_o + \tilde{\mathbf{h}}_{Ro}^H \mathbf{\Theta}_o \tilde{\mathbf{h}}_{br})\mathbf{g}_o\right\|^2. \quad (7)$$

C. Channel Statistical Properties

In this subsection, the channel statistical properties of cascade Rician channels are provided, which will be employed to analyze outage behaviors under RIS-U-NOMA framework in the following sections. On the basis of the above discussions, the channel coefficient $\tilde{h}_{brq}$ and $\tilde{h}_{R\mu qk}$ follow Rician distribution, whose PDF and CDF can be obtained from [43]. In order to attain superior performance, the coherent phase shifting scheme is selected to deal with the cascade Rician channels. As a further development, the PDF of cascade Rician fading channels from the BS to the RIS, and then to user μ, i.e., $f_{|\tilde{h}_{R\mu qk}\tilde{h}_{brq}|}$ can be given by [44]

$$f_{|\tilde{h}_{R\mu qk}\tilde{h}_{brq}|}(x) = \sum_{i=0}^{\infty}\sum_{j=0}^{\infty} \frac{4x^{i+j+1}(\kappa+1)^{i+j+2}\kappa^{i+j}}{(i!)^2(j!)^2 e^{2\kappa}} \times \left(\zeta_{br}\zeta_{R\mu}\right)^{-\frac{i+l}{2}-1} K_{i-j}\left[\frac{2x(\kappa+1)}{\sqrt{\zeta_{br}\zeta_{R\mu}}}\right], \quad (8)$$

where $\zeta_{br} = \eta d_{br}^{-\alpha}$, $\zeta_{R\mu} = \eta d_{R\mu}^{-\alpha}$, respectively. And $K_v(\cdot)$ denotes the modified Bessel function of the second kind with order v [45, Eq. (8.432)]. For notational simplicity, we denote $Y_{qk} = \left|\tilde{h}_{R\mu qk}\tilde{h}_{brq}\right|$. The mean and variance of Y_{qk} can be obtained as

$$\mathbb{E}(Y_{qk}) = \frac{\pi\sqrt{\zeta_{br}\zeta_{R\mu}}}{4(\kappa+1)}\left[L_{\frac{1}{2}}(-\kappa)\right]^2, \quad (9)$$

and

$$\mathbb{D}(Y_{qk}) = \zeta_{br}\zeta_{R\mu}\left\{1 - \frac{\pi^2}{16(1+\kappa)^2}\left[L_{\frac{1}{2}}(-\kappa)\right]^4\right\}, \quad (10)$$

respectively, where $L_{\frac{1}{2}}(\cdot)$ is the Laguerre polynomial and can be written as $L_{\frac{1}{2}}(\kappa) = e^{\frac{1}{2}}\left[(1-\kappa)K_0\left(-\frac{\kappa}{2}\right) - \kappa K_1\left(-\frac{\kappa}{2}\right)\right]$.

III. Outage Probability

In this section, the outage probability is chosen as the metric to reveal the performance of the RIS-U-NOMA networks. The approximated and asymptotic expressions of user n with ipSIC/pSIC and user m are derived in detail. According to the approximated results, we obtain the diversity orders of user n with ipSIC/pSIC and user m at high SNRs.

A. The Outage Probability of User n

For the nearby user n, it can communicate successfully with the BS in the following two steps:

- The user n decodes and subtracts the signal of the user m.
- The user n decodes its own signal without interference from x_m.

Therefore, user n will be interrupted when either of these two steps fails to decode, and the outage probability of user n in RIS-U-NOMA networks can be expressed as

$$P_n = 1 - \Pr\left(\gamma_{n\to m} > \varepsilon_m, \gamma_n > \varepsilon_n\right), \tag{11}$$

where $\varepsilon_m = 2^{R_m} - 1$ and $\varepsilon_n = 2^{R_n} - 1$ represent the target SNRs of user m and user n, respectively. The following theorem provide the outage probability of user n in the case of ipSIC.

Theorem 1. *The approximated expression of outage probability for user n with ipSIC for RIS-CD-NOMA networks can be given by*

$$P_{n,ipSIC}^{RIS-CD} \approx \sum_{u=1}^{U} A_u \frac{x_u^{Q-1}}{(Q-1)!} \gamma\left(\frac{Q\mu_{Z,n}^2}{\sigma_{Z,n}^2}, \frac{\sqrt{Q\chi}\mu_{Z,n}}{\sigma_{Z,n}^2}\right) \times \left[\Gamma\left(\frac{Q\mu_{Z,n}^2}{\sigma_{Z,n}^2}\right)\right]^{-1}, \tag{12}$$

where $\chi = \xi\left(\psi x_u \Omega_{LI}\rho + 1\right)$, $\xi \triangleq \max\left(\tau, \beta\right)$, $\tau = \frac{\varepsilon_m}{\rho(a_m - \varepsilon_m a_n)}$ with $a_m > \varepsilon_m a_n$ and $\beta = \frac{\varepsilon_n}{a_n \rho}$. With the case of ipSIC, we can apply $\psi = 1$. $\mu_{Z,n} = \frac{\sqrt{\pi\zeta_{Bn}}}{2} + \sqrt{\zeta_{br}\zeta_{Rn}}\frac{\sigma_{cc}^2\Gamma\left((K\mu_{cc}^2+\sigma_{cc}^2)(\sigma_{cc}^2)^{-1}\right)}{\mu_{cc}\Gamma\left(K\mu_{cc}^2(\sigma_{cc}^2)^{-1}\right)}$ and $\sigma_{Z,n}^2 = \zeta_{Bn} + \zeta_{br}\zeta_{Rn}\frac{(\sigma_{cc}^2)^2\Gamma\left((K\mu_{cc}^2+2\sigma_{cc}^2)(\sigma_{cc}^2)^{-1}\right)}{\mu_{cc}^2\Gamma\left(K\mu_{cc}^2(\sigma_{cc}^2)^{-1}\right)} + \frac{\sqrt{\zeta_{Bn}\zeta_{br}\zeta_{Rn}}\sigma_{cc}^2\Gamma\left((K\mu_{cc}^2+\sigma_{cc}^2)(\sigma_{cc}^2)^{-1}\right)}{\mu_{cc}\Gamma\left(K\mu_{cc}^2(\sigma_{cc}^2)^{-1}\right)} - (\mu_{Z,n})^2$. μ_{cc} and σ_{cc}^2 are mean and variance of the cascade channel obtained from Section II.C, respectively, which can be given by $\mu_{cc} = \frac{\pi}{4(\kappa+1)}\left[L_{\frac{1}{2}}(-\kappa)\right]^2$ and $\sigma_{cc}^2 = 1 - \frac{\pi^2}{16(\kappa+1)^2}\left[L_{\frac{1}{2}}(\kappa)\right]^4$. The lower incomplete Gamma function is expressed as $\gamma(a,x) = \int_0^x t^{a-1}e^{-t}dt$ and $\Gamma(\cdot)$ denotes the gamma function [45, Eq. (8.310.1)]. x_u and A_u are the abscissas and weight of Gauss-Laguerre quadrature, respectively. In particularly, x_u is the u-th zero point of Laguerre polynomial $L_U(x_u)$ and the u-th weight can be expressed as $H_u = \frac{(U!)^2 x_u}{[L_{U+1}(x_u)]^2}$. In addition, U is the parameter to guarantee a complexity-accuracy tradeoff.

Proof. See Appendix A. □

Corollary 1. *For the special case of $\psi = 0$, the approximated expression of outage probability for user n in RIS-CD-NOMA networks can be represented as*

$$P_{n,pSIC}^{RIS-CD} \approx \sum_{u=1}^{U} A_u \frac{x_u^{Q-1}}{(Q-1)!} \gamma\left(\frac{Q\mu_Z^2}{\sigma_Z^2}, \frac{\sqrt{Q\xi}\mu_Z}{\sigma_Z^2}\right) \times \left[\Gamma\left(\frac{Q\mu_Z^2}{\sigma_Z^2}\right)\right]^{-1}. \tag{13}$$

Proof. Upon substituting $\psi = 0$ into (12) and applying similar processes, the outage probability of user n with pSIC can be written as

$$P_{n,pSIC}^{RIS-CD} = \frac{2(\kappa+1)}{\Gamma(\varphi_n+1)\alpha_{sn}e^{\kappa}} \int_0^{\sqrt{\xi}} x e^{-(\kappa+1)\frac{x^2}{\alpha_{sn}}} \times K_0\left(2x\sqrt{\frac{\kappa(\kappa+1)}{\alpha_{sn}}}\right)\gamma\left(\varphi_n+1, \frac{\sqrt{\xi}-x}{\phi_n}\right)dx. \tag{14}$$

By further applying Gaussian-Chebyshev quadrature into the above integral expression, we can obtain (13). The proof is completed. □

Corollary 2. *For the special case with $Q = 1$, the approximated expression of outage probability for user n with ipSIC/pSIC for RIS-PD-NOMA networks can be expressed as*

$$P_{n,ipSIC}^{RIS-PD} \approx \sum_{u=1}^{U} A_u \gamma\left(\frac{\mu_Z^2}{\sigma_Z^2}, \frac{\sqrt{\xi\left(x_u\Omega_{LI}\rho+1\right)}\mu_Z}{\sigma_Z^2}\right) \times \left[\Gamma\left(\frac{\mu_Z^2}{\sigma_Z^2}\right)\right]^{-1}, \tag{15}$$

and

$$P_{n,pSIC}^{RIS-PD} \approx \sum_{u=1}^{U} A_u \gamma\left(\frac{\mu_Z^2}{\sigma_Z^2}, \frac{\sqrt{\xi}\mu_Z}{\sigma_Z^2}\right)\left[\Gamma\left(\frac{\mu_Z^2}{\sigma_Z^2}\right)\right]^{-1}, \tag{16}$$

respectively.

B. The Outage Probability of User m

Based on the NOMA principle, if the user m can't decode its own information from the signals received, the communication of the user m will be interrupted. In this case, the corresponding outage probability can be given by

$$P_m = \Pr\left(\gamma_m < \varepsilon_m\right), \tag{17}$$

where $\varepsilon_m = 2^{R_m} - 1$ and R_m is the target rate.

Theorem 2. *The approximated expression of outage probability for user m in RIS-CD-NOMA networks can be given by*

$$P_m^{RIS-CD} = \left[\Gamma\left(\frac{Q\mu_{Z,m}^2}{\sigma_{Z,m}^2}\right)\right]^{-1}\gamma\left(\frac{Q\mu_{Z,m}^2}{\sigma_{Z,m}^2}, \frac{\sqrt{Q\tau}\mu_{Z,m}}{\sigma_{Z,m}^2}\right), \tag{18}$$

where $\mu_{Z,m} = \frac{\sqrt{\pi\zeta_{Bm}}}{2} + \sqrt{\zeta_{br}\zeta_{Rm}}\frac{\sigma_{cc}^2\Gamma\left((K\mu_{cc}^2+\sigma_{cc}^2)(\sigma_{cc}^2)^{-1}\right)}{\mu_{cc}\Gamma\left(K\mu_{cc}^2(\sigma_{cc}^2)^{-1}\right)}$ and $\sigma_{Z,m}^2 = \zeta_{Bm} + \zeta_{br}\zeta_{Rm}\frac{(\sigma_{cc}^2)^2\Gamma\left((K\mu_{cc}^2+2\sigma_{cc}^2)(\sigma_{cc}^2)^{-1}\right)}{\mu_{cc}^2\Gamma\left(K\mu_{cc}^2(\sigma_{cc}^2)^{-1}\right)} + \frac{\sqrt{\zeta_{Bm}\zeta_{br}\zeta_{Rm}}\sigma_{cc}^2\Gamma\left((K\mu_{cc}^2+\sigma_{cc}^2)(\sigma_{cc}^2)^{-1}\right)}{\mu_{cc}\Gamma\left(K\mu_{cc}^2(\sigma_{cc}^2)^{-1}\right)} - (\mu_{Z,m})^2$. μ_{cc} and σ_{cc}^2 are mean and variance of the cascade channel, which can be represent as $\mu_{cc} = \frac{\pi}{4(\kappa+1)}\left[L_{\frac{1}{2}}(-\kappa)\right]^2$ and $\sigma_{cc}^2 = 1 - \frac{\pi^2}{16(\kappa+1)^2}\left[L_{\frac{1}{2}}(\kappa)\right]^4$. $\tau = \frac{\varepsilon_m}{\rho(a_m - \varepsilon_m a_n)}$ is a variant of user m's target SNR.

Proof. See Appendix B. □

Corollary 3. *For the special case with $Q = 1$, the approximated expression of outage probability for user m in RIS-PD-NOMA networks can be written as*

$$P_m^{RIS-PD} = \left[\Gamma\left(\frac{\mu_Z^2}{\sigma_Z^2}\right)\right]^{-1} \gamma\left(\frac{\mu_Z^2}{\sigma_Z^2}, \frac{\sqrt{\tau}\mu_Z}{\sigma_Z^2}\right). \tag{19}$$

Proposition 1. *According to above analyses, the system outage probability of RIS-CD-NOMA and RIS-PD-NOMA can be given by*

$$P_{\varpi}^{RIS-CD} = 1 - \left(1 - P_{n,\varpi}^{RIS-CD}\right)\left(1 - P_m^{RIS-CD}\right), \tag{20}$$

and

$$P_{\varpi}^{RIS-PD} = 1 - \left(1 - P_{n,\varpi}^{RIS-PD}\right)\left(1 - P_m^{RIS-PD}\right), \tag{21}$$

where $\varpi \in \{ipSIC, pSIC\}$. $P_{n,ipSIC}^{RIS-CD}$, $P_{n,pSIC}^{RIS-CD}$ and P_m^{RIS-CD} are given by (12), (13) *and* (18)*, respectively. $P_{n,ipSIC}^{RIS-PD}$, $P_{n,pSIC}^{RIS-PD}$ and P_m^{RIS-PD} can be obtained from* (15), (16) *and* (19)*, respectively.*

C. The Outage Probability of RIS-OMA

For RIS-OMA networks, the communication process of a pair of users is completed in two time slots. In each time slot, the BS communicates with one of orthogonal users. In this case, we can define the outage probability as the received SNR, i.e., γ_o^{OMA}, falls bellow the target SNR, which we can express as

$$P_o^{OMA} = \Pr\left(\gamma_o^{OMA} < \varepsilon_o^{OMA}\right), \tag{22}$$

where $\varepsilon_o^{OMA} = 2^{2R_o^{OMA}} - 1$ denotes the threshold SNR of user o to detect the signal x_o. Similar to the above derivation process, we can get the outage probability of user o in the following theorem.

Theorem 3. *The approximated expression of outage probability for user o in RIS-OMA networks can be given by*

$$P_o^{OMA} = \left[\Gamma\left(\frac{Q\mu_Z^2}{\sigma_Z^2}\right)\right]^{-1} \gamma\left(\frac{Q\mu_Z^2}{\sigma_Z^2}, \frac{\sqrt{Q\xi_o}\mu_Z}{\sigma_Z^2}\right), \tag{23}$$

where $\xi_o = \frac{\varepsilon_o^{OMA}}{\rho}$.

Proof. Upon substituting (7) into (22), the outage probability of user o can be given by

$$P_o^{OMA} = \Pr\left[\underbrace{\left\|diag(\mathbf{h}_o + \widetilde{\mathbf{h}}_{Ro}^H \mathbf{\Theta}_o \widetilde{\mathbf{h}}_{br})\mathbf{g}_o\right\|^2}_{Z_o} < \frac{\varepsilon_o^{OMA}}{\rho}\right]. \tag{24}$$

Due to two time slots are required to complete the transmission of near and far users in RIS-OMA networks, we denote the target SNR for user o as $\varepsilon_o^{OMA} = 2^{2R_o^{OMA}} - 1$. From the outcome in Appendix A, the CDF of Z_o can be represent as

$$F_{Z_o}(z) \approx [\Gamma(\varphi_z + 1)]^{-1} \gamma\left(\varphi_z + 1, \frac{\sqrt{Qz}}{\phi_z}\right), \tag{25}$$

Applying (25) into (24), the expression in (23) can be obtained. The proof is completed.

□

Proposition 2. *Similar to* (21)*, the system outage probability of RIS-OMA can be written as*

$$P_{OMA} = 1 - \prod_o \left(1 - P_o^{OMA}\right), \tag{26}$$

where P_o^{OMA} is given by (23)*.*

D. Diversity Order Analysis

For the purpose of gaining better insights, the diversity order is an important parameter to evaluate the outage performance. It can express the slope and trend of the curves as SNR changes. Precisely speaking, the diversity order is defined as

$$D = -\lim_{\rho \to \infty} \frac{\log\left(P^{\infty}(\rho)\right)}{\log \rho}, \tag{27}$$

where $P^{\infty}(\rho)$ denotes the asymptotic outage probability at high SNRs.

Corollary 4. *When $\rho \to \infty$, the asymptotic expression for outage probability of user n with ipSIC can be given by*

$$P_{n,ipSIC}^{\infty} = \sum_{u=1}^{U} A_u \frac{x_u^{Q-1}}{(Q-1)!} \gamma\left(\frac{Q\mu_Z^2}{\sigma_Z^2}, \frac{\sqrt{Q\tilde{\chi}}\mu_Z}{\sigma_Z^2}\right) \times \left[\Gamma\left(\frac{Q\mu_Z^2}{\sigma_Z^2}\right)\right]^{-1}, \tag{28}$$

where $\tilde{\chi} = \lim_{\rho \to \infty} \xi\left(\psi x_u \Omega_{LI} \rho + 1\right) \approx x_u \Omega_{LI} \rho \xi$, $\xi \triangleq \max(\tau, \beta)$, $\tau = \frac{\varepsilon_m}{\rho(a_m - \varepsilon_m a_n)}$ and $\beta = \frac{\varepsilon_n}{a_n \rho}$.

Remark 1. *Upon substituting* (28) *into* (27)*, user n achieves zero diversity order as ipSIC applied, which leads to the same conclusion as traditional NOMA communication. It is caused by the effect of residual interference.*

Corollary 5. *When $\rho \to \infty$, the asymptotic expression for outage probability of user n with pSIC can be given by*

$$P_{n,pSIC}^{\infty} = \sum_{u=1}^{U} A_u \frac{x_u^{Q-1}}{(Q-1)!} \gamma\left(\frac{Q\mu_Z^2}{\sigma_Z^2}, \frac{\sqrt{Q\xi}\mu_Z}{\sigma_Z^2}\right) \times \left[\Gamma(\frac{Q\mu_Z^2}{\sigma_Z^2})\right]^{-1}, \tag{29}$$

Remark 2. *Substituting* (29) *into* (27)*, the diversity order of user n with pSIC can be achieved by $\frac{Q\mu_n^2}{2\sigma_n^2}$, which is in connection with Q, K and κ. For the case with $Q = 1$, the diversity order of user n with pSIC can be obtained by $\frac{\mu_n^2}{2\sigma_n^2}$, which is related to the parameters K and κ.*

Corollary 6. *When $\rho \to \infty$, the asymptotic expression for outage probability of user m is given by*

$$P_m^{\infty} = \left[\Gamma\left(\frac{Q\mu_Z^2}{\sigma_Z^2}\right)\right]^{-1} \frac{\sigma_Z^2}{Q\mu_Z^2} \left(\frac{\sqrt{Q\tau}\mu_Z}{\sigma_Z^2}\right)^{\frac{Q\mu_Z^2}{\sigma_Z^2}}. \tag{30}$$

Proof. According to the series representation $\gamma(\alpha,x)=\sum_{n=0}^{\infty}\frac{(-1)^n x^{\alpha+n}}{n!(\alpha+n)}$ [45, Eq. (8.354.1)], as ρ tends to infinity, i.e., $\tau\to 0$, we can approximate $\gamma(\frac{Q\mu_Z^2}{\sigma_Z^2},\frac{\sqrt{Q\tau}\mu_Z}{\sigma_Z^2})$ with the first term of the series, which can be expressed as

$$\gamma\left(\frac{Q\mu_Z^2}{\sigma_Z^2},\frac{\sqrt{Q\tau}\mu_Z}{\sigma_Z^2}\right)\approx\frac{\sigma_Z^2}{Q\mu_Z^2}\left(\frac{\sqrt{Q\tau}\mu_Z}{\sigma_Z^2}\right)^{\frac{Q\mu_Z^2}{\sigma_Z^2}}. \tag{31}$$

Substitute (31) into (18) to obtain (30). The proof is completed. □

Remark 3. *Substituting* (30) *into* (27)*, the diversity order of user m can be obtained by $\frac{Q\mu_m^2}{2\sigma_m^2}$, which is obviously related to the number of subcarriers Q, RIS elements number K and Rician factor κ. For the special case with $Q=1$, i.e., RIS-PD-NOMA, the diversity order of user m can be obtained by $\frac{\mu_m^2}{2\sigma_m^2}$, which is related to the parameters K and κ.*

IV. Ergodic Rate

In this section, the performance of ergodic rate for user n and user m for RIS-U-NOMA networks will be analyzed. For a more comprehensive analysis, we consider both the ipSIC/pSIC cases.

For the nearby user n, the ergodic rate can be given by

$$R_n^{erg}=\mathbb{E}\left[\log\left(1+\frac{\rho\left\|diag(\mathbf{h}_n+\widetilde{\mathbf{h}}_{Rn}^H\mathbf{\Theta}_n\widetilde{\mathbf{h}}_{br})\mathbf{g}_n\right\|^2 a_n}{\psi\rho\|\mathbf{h_I}\|^2+1}\right)\right], \tag{32}$$

where $\psi=0,1$ denote pSIC and ipSIC, respectively. It is worth pointing out that when $\psi=1$, it is difficult to obtain the ergodic rate expression. We can use simulation software to numerically evaluate this situation in the next section. In addition, the following theorem will focus on the ergodic rate for user n with pSIC.

Theorem 4. *The ergodic rate for user n with pSIC for RIS-CD-NOMA networks can be simplified to the form as* (33) *at the top of next page.*

Proof. By substituting $\psi=0$ into (32), the ergodic rate of user n with pSIC can be calculated as

$$\begin{aligned}R_{n,pSIC}^{erg,CD}=&\mathbb{E}\left[\log\left(1+\underbrace{\left\|diag(\mathbf{h}_n+\tilde{\mathbf{h}}_{Rn}^H\mathbf{\Theta}_n\tilde{\mathbf{h}}_{br})\mathbf{g}_n\right\|^2}_{Z_1}\rho a_n\right)\right]\\=&\frac{\rho a_n}{\ln 2}\int_0^{\infty}\frac{1-F_{Z_1}(x)}{1+\rho a_n x}dx.\end{aligned} \tag{34}$$

By the virtue of (13), the CDF of Z_1 can be represented as

$$\begin{aligned}F_{Z_1}(x)\approx&\sum_{u=1}^{U}A_u\frac{x_u^{Q-1}}{(Q-1)!}\gamma\left(\frac{Q\mu_Z^2}{\sigma_Z^2},\frac{\sqrt{Qx}\mu_Z}{\sigma_Z^2}\right)\\&\times\left[\Gamma\left(\frac{Q\mu_Z^2}{\sigma_Z^2}\right)\right]^{-1}.\end{aligned} \tag{35}$$

Substituting (35) into (34), (33) can be obtained. The proof is completed. □

Corollary 7. *For the special case with $Q=1$, the ergodic rate for user n with pSIC for RIS-PD-NOMA networks can be expressed as* (36) *at the top of next page.*

The ergodic rate for user m will be affected by the signal of user n, which can be expressed by the following theorem.

Theorem 5. *The ergodic rate for user m in RIS-CD-NOMA networks can be given by*

$$\begin{aligned}R_m^{erg,CD}=&\frac{1}{\ln 2}\int_0^{\frac{a_m}{a_n}}\frac{1}{1+x}-\left[(1+x)\Gamma\left(\frac{Q\mu_Z^2}{\sigma_Z^2}\right)\right]^{-1}\\&\times\gamma\left(\frac{Q\mu_Z^2}{\sigma_Z^2},\frac{\mu_Z}{\sigma_Z^2}\sqrt{\frac{Qx}{\rho\left(a_m-xa_n\right)}}\right)dx.\end{aligned} \tag{37}$$

Proof. See Appendix C. □

Corollary 8. *For the special case with $Q=1$, the ergodic rate for user m in RIS-PD-NOMA networks can be expressed as*

$$\begin{aligned}R_m^{erg,PD}=&\frac{1}{\ln 2}\int_0^{\frac{a_m}{a_n}}\frac{1}{1+x}-\left[(1+x)\Gamma\left(\frac{\mu_Z^2}{\sigma_Z^2}\right)\right]^{-1}\\&\times\gamma\left(\frac{\mu_Z^2}{\sigma_Z^2},\frac{\mu_Z}{\sigma_Z^2}\sqrt{\frac{x}{\rho\left(a_m-xa_n\right)}}\right)dx.\end{aligned} \tag{38}$$

As for RIS-OMA networks, the expression of achievable data rate can be written as $R_o^{OMA}=\frac{1}{2}\log\left(1+\gamma_o^{OMA}\right)$. Referring to the derivation processes of (34), the expression of ergodic rate for user o can be provided in the following corollary.

Corollary 9. *The ergodic rate expression for user o in RIS-OMA networks can be given by*

$$R_{o,OMA}^{erg}=\frac{\rho}{2\ln 2}\int_0^{\infty}\frac{\Gamma\left(\frac{Q\mu_Z^2}{\sigma_Z^2}\right)-\gamma\left(\frac{Q\mu_Z^2}{\sigma_Z^2},\frac{\sqrt{Qx}\mu_Z}{\sigma_Z^2}\right)}{\Gamma\left(\frac{Q\mu_Z^2}{\sigma_Z^2}\right)(1+\rho x)}dx. \tag{39}$$

A. Slope Analysis

Resemble the diversity order, the slope of the performance curve at high SNRs is another performance evaluation metric, which is designed to highlight the diversity in ergodic rate. Therefore, the slope of the ergodic rate can be defined as

$$S=\lim_{\rho\to\infty}\frac{R_{erg}^{\infty}(\rho)}{\log(\rho)}, \tag{40}$$

where $R_{erg}^{\infty}(\rho)$ is the approximated ergodic rate in high SNR region.

It can be observed from (33) that it is difficult to calculate the asyptotic expression of the ergodic rate at high SNRs. To advance further analysis, we try to apply Jensen Inequality to obtain the following theorem for the upper bound of ergodic rate.

$$R_{n,pSIC}^{erg,CD} = \frac{\rho a_n}{\ln 2}\int_0^{\infty}(1+\rho a_n x)^{-1}\left\{1-\sum_{u=1}^{U}A_u\frac{x_u^{Q-1}}{(Q-1)!}\gamma\left(\frac{Q\mu_Z^2}{\sigma_Z^2},\frac{\sqrt{Qx}\mu_Z}{\sigma_Z^2}\right)\left[\Gamma\left(\frac{Q\mu_Z^2}{\sigma_Z^2}\right)\right]^{-1}\right\}dx. \quad (33)$$

$$R_{n,pSIC}^{erg,PD} = \frac{\rho a_n}{\ln 2}\int_0^{\infty}(1+\rho a_n x)^{-1}\left\{1-\sum_{u=1}^{U}A_u\gamma\left(\frac{\mu_Z^2}{\sigma_Z^2},\frac{\sqrt{x}\mu_Z}{\sigma_Z^2}\right)\left[\Gamma\left(\frac{\mu_Z^2}{\sigma_Z^2}\right)\right]^{-1}\right\}dx. \quad (36)$$

Theorem 6. *The upper bound of ergodic rate for user n with pSIC for RIS-CD-NOMA networks can be obtained as*

$$R_{n,pSIC}^{upp,CD} = \log\left[1+\rho a_n Q\left(\zeta_{Bn}+\frac{\sigma_Z^4}{\mu_Z^2}\zeta_{br}\zeta_{Rn}\frac{\Gamma\left(\frac{K\mu_Z^2}{\sigma_Z^2}+2\right)}{\Gamma\left(\frac{K\mu_Z^2}{\sigma_Z^2}\right)}+\sqrt{\pi\zeta_{Bn}\zeta_{br}\zeta_{Rn}}\frac{\sigma_Z^2}{\mu_Z}\frac{\Gamma\left(\frac{K\mu_Z^2}{\sigma_Z^2}+1\right)}{\Gamma\left(\frac{K\mu_Z^2}{\sigma_Z^2}\right)}\right)\right], \quad (41)$$

where $\mu_Z = \frac{\sqrt{\pi\zeta_{Bn}}}{2}+\sqrt{\zeta_{br}\zeta_{Rn}}\frac{\sigma_{cc}^2\Gamma\left((K\mu_{cc}^2+\sigma_{cc}^2)(\sigma_{cc}^2)^{-1}\right)}{\mu_{cc}\Gamma\left(K\mu_{cc}^2(\sigma_{cc}^2)^{-1}\right)}$ *and* $\sigma_Z^2 = \zeta_{Bn}+\zeta_{br}\zeta_{Rn}\frac{(\sigma_{cc}^2)^2\Gamma\left((K\mu_{cc}^2+2\sigma_{cc}^2)(\sigma_{cc}^2)^{-1}\right)}{\mu_{cc}^2\Gamma\left(K\mu_{cc}^2(\sigma_{cc}^2)^{-1}\right)}+\frac{\sqrt{\zeta_{Bn}\zeta_{br}\zeta_{Rn}}\sigma_{cc}^2\Gamma\left((K\mu_{cc}^2+\sigma_{cc}^2)(\sigma_{cc}^2)^{-1}\right)}{\mu_{cc}\Gamma\left(K\mu_{cc}^2(\sigma_{cc}^2)^{-1}\right)}-(\mu_Z)^2$.

Proof. With the assistance of (34) and Jensen Inequality, the upper bound of ergodic rate can be written as

$$R_{n,pSIC}^{erg,CD} = \mathbb{E}\left[\log\left(1+\left\|diag(\mathbf{h}_n+\widetilde{\mathbf{h}}_{Rn}^H\mathbf{\Theta}_n\widetilde{\mathbf{h}}_{br})\mathbf{g}_n\right\|^2\rho a_n\right)\right] \le \log\left[1+\rho a_n\mathbb{E}\left(\underbrace{\left\|diag(\mathbf{h}_n+\widetilde{\mathbf{h}}_{Rn}^H\mathbf{\Theta}_n\widetilde{\mathbf{h}}_{br})\mathbf{g}_n\right\|^2}_{Y}\right)\right]. \quad (42)$$

On the basis of (9), (10) and [43, Eq. (2.16)], we can achieve the expectation of Y. After some mathematical manipulations, (41) can be obtained. The proof is completed. □

Corollary 10. *For the special case with $Q = 1$, the upper bound of ergodic rate for user n with pSIC for RIS-PD-NOMA networks can be given by*

$$R_{n,pSIC}^{upp,PD} = \log\left[1+\rho a_n\left(\zeta_{Bn}+\frac{\sigma_Z^4}{\mu_Z^2}\zeta_{br}\zeta_{Rn}\frac{\Gamma\left(\frac{K\mu_Z^2}{\sigma_Z^2}+2\right)}{\Gamma\left(\frac{K\mu_Z^2}{\sigma_Z^2}\right)}+\sqrt{\pi\zeta_{Bn}\zeta_{br}\zeta_{Rn}}\frac{\sigma_Z^2}{\mu_Z}\frac{\Gamma\left(\frac{K\mu_Z^2}{\sigma_Z^2}+1\right)}{\Gamma\left(\frac{K\mu_Z^2}{\sigma_Z^2}\right)}\right)\right]. \quad (43)$$

Remark 4. *Upon substituting* (41) *into* (40)*, the slope of user n with pSIC at high SNRs is equal to one, which comes to a consistent conclusion with conventional RIS-NOMA networks. It shows that the high SNR slope won't be improved by the direct link between BS and user n.*

TABLE I: Summary of Diversity order and Slope at high SNRs

Type	Q	User	SIC	D	S
RIS-OMA	——	o	——	$\frac{Q\mu_o^2}{2\sigma_o^2}$	$\frac{1}{2}$
RIS-U-NOMA	$Q=1$	m	——	$\frac{\mu_m^2}{2\sigma_m^2}$	0
		n	ipSIC	0	—
			pSIC	$\frac{\mu_n^2}{2\sigma_n^2}$	1
	$Q>1$	m	——	$\frac{Q\mu_m^2}{2\sigma_m^2}$	0
		n	ipSIC	0	—
			pSIC	$\frac{Q\mu_n^2}{2\sigma_n^2}$	1

When $\rho\to\infty$, the asymptotic expression of ergodic rate for user m in RIS-U-NOMA networks can be given by

$$R_{m,erg}^{\infty} = \log\left[1+\left(\frac{a_m}{a_n}\right)\right]. \quad (44)$$

Remark 5. *By substituting* (44) *into* (40)*, the numerical value of high SNR slope of user m is zero.*

Corollary 11. *For RIS-OMA networks, the upper bound of ergodic rate for user o can be represented by*

$$R_{o,OMA}^{upp} = \frac{1}{2}\log\left[1+\rho N\left(\zeta_{B\mu}+\frac{\sigma_Z^4}{\mu_Z^2}\zeta_{br}\zeta_{R\mu}\frac{\Gamma\left(\frac{K\mu_Z^2}{\sigma_Z^2}+2\right)}{\Gamma\left(\frac{K\mu_Z^2}{\sigma_Z^2}\right)}+\sqrt{\pi\zeta_{B\mu}\zeta_{br}\zeta_{R\mu}}\frac{\sigma_Z^2}{\mu_Z}\frac{\Gamma\left(\frac{K\mu_Z^2}{\sigma_Z^2}+1\right)}{\Gamma\left(\frac{K\mu_Z^2}{\sigma_Z^2}\right)}\right)\right]. \quad (45)$$

Remark 6. *Substituting* (45) *into* (40)*, the high SNR slope for RIS-OMA networks is obtained to be $\frac{1}{2}$.*

The relationship between different factors and metrics are summarized in TABLE I, where we use "Q" , "D" and "S" to represent the number of subcarriers, diversity order and slope in high SNR regime, respectively.

B. System throughput

In delay-limited transmission scenario, to observe the system throughput, we could appraise the outage probability performance at a constant transmission rate, i.e., R_n and R_m [38]. As for delay-tolerant mode, the throughput is affected by the constant transmission rate sent by the BS. As a consequence, the delay-limited and delay-tolerant system throughput for RIS-U-NOMA networks can be given by

$$R_{dl,\Lambda}^{\Xi} = \left(1-P_{n,\Lambda}^{\Xi}\right)R_n+\left(1-P_m^{\Xi}\right)R_m, \quad (46)$$

TABLE II: The parameters for simulation results

Monte Carlo simulations repeated	10^7 iterations
Power allocation factors in BS	$a_m = 0.8$ $a_n = 0.2$
Target data rates	$R_m = 0.1 \sim 1$ BPCU $R_n = 0.1 \sim 1$ BPCU
Distance from BS to user m	10 m
Distance from BS to user n	8 m
Distance from BS to RIS	5 m
Distance from RIS to user m	6 m
Distance from RIS to user n	4 m
Pass loss exponent	$\alpha = 2$

and

$$R_{dt}^{\Xi} = R_m^{erg,\Xi} + R_{n,pSIC}^{erg,\Xi}, \tag{47}$$

respectively. $\Xi \in \{CD, PD\}$. $P_{n,ipSIC}^{CD}$, $P_{n,pSIC}^{CD}$, $P_{n,ipSIC}^{PD}$ and $P_{n,pSIC}^{PD}$ can be obtained from (12), (13), (15) and (16), respectively. According to (18) and (19), P_m^{CD} and P_m^{PD} can be achieved. And $R_{n,pSIC}^{erg,CD}$,$R_{n,pSIC}^{erg,PD}$, $R_m^{erg,CD}$ and $R_m^{erg,PD}$ can be substituted from (33), (36), (37) and (38), respectively.

V. Simulation Results

In this section, we utilize Monte Carlo simulation to verify the results of performance analysis derived for the RIS-U-NOMA networks in the previous sections. The simulation parameters used in this section are summarized in Table II. For notational simplicity, BPCU is used to denote bit per channel use. To ensure the accuracy of the conclusion, the complexity-accuracy trade-off parameter U is set to be $U = 50$. We select different values of subcarrier number Q, configurable elements K and Rician factor κ to analyze the effects of the parameters. Also, the variations of BPCU and path loss α are within our consideration. For comparison purposes, RIS-OMA and FD/HD-DF relays are selected as benchmarks.

A. Outage Probability

To reflect the superiority of RIS-U-NOMA networks, Fig. 2 plots the outage probability versus SNR with different values of residual interference and benchmarks, with a target rate of $R_m = 0.5$ and $R_n = 0.5$ BPCU. The parameters of subcarrier number, Rician factor and configurable elements are $Q = 2$, $\kappa = -10$ dB and $K = 50$, respectively. Based on (12) and (13), the outage probability for user n with ipSIC/pSIC are plotted by the circle and exact right triangle curves, respectively. The corresponding curves of user m are plotted by exact diamond solid according to (18). The plus sign solid line for outage probability of user o in RIS-OMA is plotted in view of (23). The simulation points shown by solid black dot are given by Monte Carlo simulation, which match well with the theoretical results. We can observe from the figure that the outage behavior of user m in RIS-U-NOMA networks is better than that of RIS-OMA and conventional FD/HD-DF relays, which are plotted by red asterisk and equilateral triangle solid line, respectively. The primary reasons can be summarized as follows: 1) RIS-U-NOMA networks can provide better user fairness, more rate-pair-selectivity and better flexibility compared with RIS-OMA; 2) The loop residual interference will have a more serious influence on FD-DF relays, and it is supposed to use efficient cancellation method to eliminate the impact; and 3) HD-DF relays are not affected by loop residual interference, but in terms of implementation, this mode sacrifices some performance. Moreover, the influence of different values of residual interference are taken into consideration. As the residual interference decreases, the outage behaviors for users n applying ipSIC becomes better, which behaves more closely with the pSIC case. However, it still converges to the error floor at high SNRs. Hence, we can conclude that user n with ipSIC has *zero* diversity order, which confirms the conclusion in **Remark 1**. From the above conclusion, it can be observed that less residual interference can reduce the outage probability of the networks. It is necessary to explore an advanced SIC method (e.g., user pair selection) to reduce the impact of residual interference on outage performance.

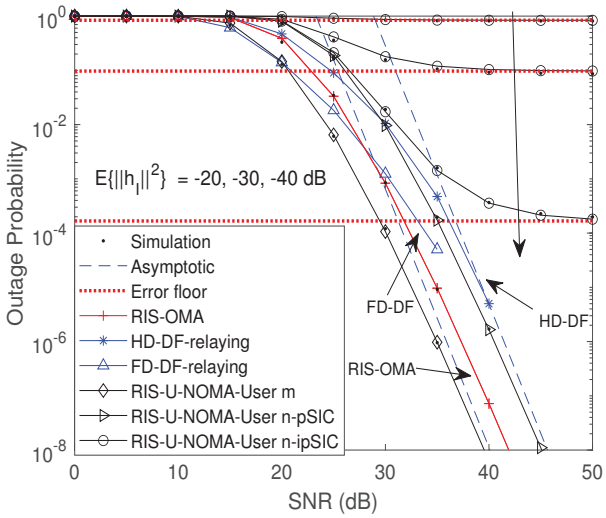

Fig. 2: Outage probability versus the transmit SNR, with $Q = 2$, $K = 50$, $\kappa = -10$ dB, $R_m = 0.5$ and $R_n = 0.5$ BPCU.

Fig. 3 plots the outage probability for RIS-U-NOMA networks versus SNR. The parameters of subcarrier number, Rician factor and residual interference are $Q = 2$, $\kappa = -10$ dB and $\mathbb{E}\{\|\mathbf{h_I}\|^2\} = -30$ dB, respectively. It can be observed that user m has better outage performance than that in RIS-OMA, while user n in the case of pSIC is inferior to that in RIS-OMA. This is due to the different power factors between two users. This conclusion is similar to that in [46] and identifies a good fairness and adaptability in the RIS-U-NOMA networks. The asymptotic outage probability for user n with ipSIC/pSIC and user m are indicated by blue dotted curve, on the basis of the results in (28), (29) and (30), respectively. It provides an efficient performance evaluation method since the asymptotic outage probability matches the exact performance curves in high SNR region. One can observe that the outage probability for user n with ipSIC converges to the error floor due to the effect of residual interference, so the diversity gain obtained in this case is *zero*. The conclusion in **Remark 1** is confirmed.

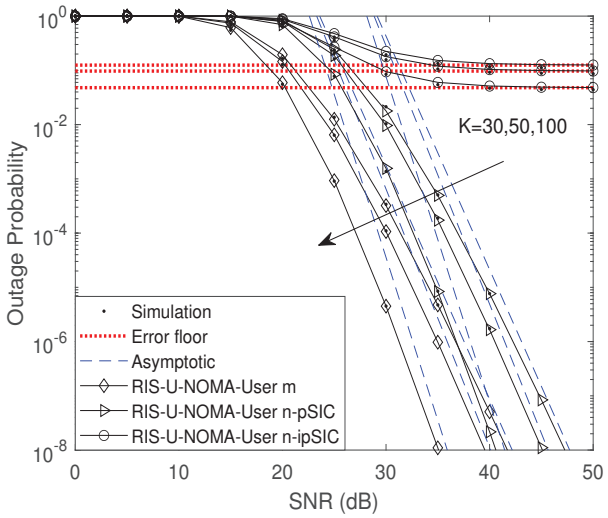

Fig. 3: Outage probability versus the transmit SNR, with $Q = 2$, $\kappa = -10$ dB, $\mathbb{E}\{\|\mathbf{h_I}\|^2\} = -30$ dB, $R_m = 0.5$ and $R_n = 0.5$ BPCU.

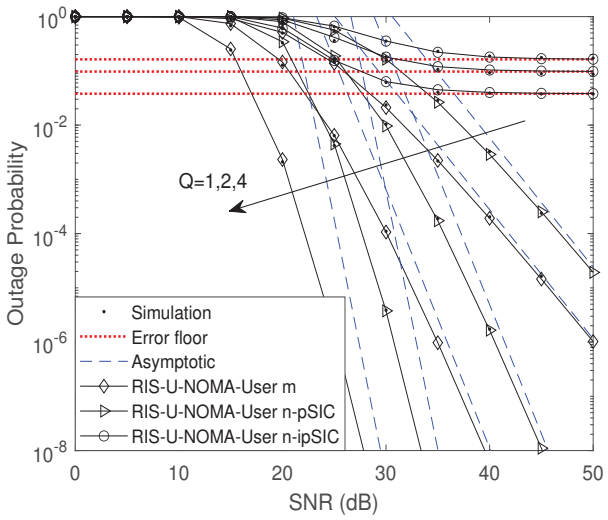

Fig. 4: Outage probability versus the transmit SNR, with $K = 50$, $\kappa = -10$ dB, $\mathbb{E}\{\|\mathbf{h_I}\|^2\} = -30$ dB, $R_m = 0.5$ and $R_n = 0.5$ BPCU.

As can be seen from the figure, with the value of K increasing from 30 to 100, the outage probability of user n and m decreases. Meantime, the slope of the asymptotic outage probability curve grows as K increasing, i.e., the diversity gain is better. This is due to the diversity order of user n with pSIC and user m are related to the RIS configurable elements, which are also obtained from the conclusions in **Remark 2** and **Remark 3**. Hence, in areas with poor channel conditions, we can set up more configurable elements to compensate for the loss of the links and satisfy different service requirements.

Additionally, Fig. 4 plots the outage probability of RIS-U-NOMA networks versus SNR with different numbers of subcarrier Q, with the setting of $\kappa = -10$ dB, $\mathbb{E}\{\|\mathbf{h_I}\|^2\} = -30$ dB, $R_m = 0.5$ and $R_n = 0.5$ BPCU. As for the case of $Q = 1$, the RIS-U-NOMA network is applied into RIS-PD-NOMA. The approximated outage probability curve of the user n in ipSIC/pSIC cases and user m for RIS-PD-NOMA are plotted by (15), (16) and (19), respectively. It is worth pointing that the asymptotic outage probability for users is similar to the analysis results under high SNR regime. In addition, as Q varies from 1 to 4, we can observe from the figure that the outage probability of users m and n is getting much smaller and asymptotic curves gain a steeper slope, i.e., the diversity order gain is better. This is because the diversity order is related to the number of subcarriers Q, which is also obtained from **Remark 2** and **Remark 3**. As for the case of ipSIC, user n has a smaller error floor as Q grows, while the diversity order gain are $zero$ in all conditions. This situation indicates that the number of subcarrier has a great impact on the performance. We can reasonably adjusted it according to actual communication needs.

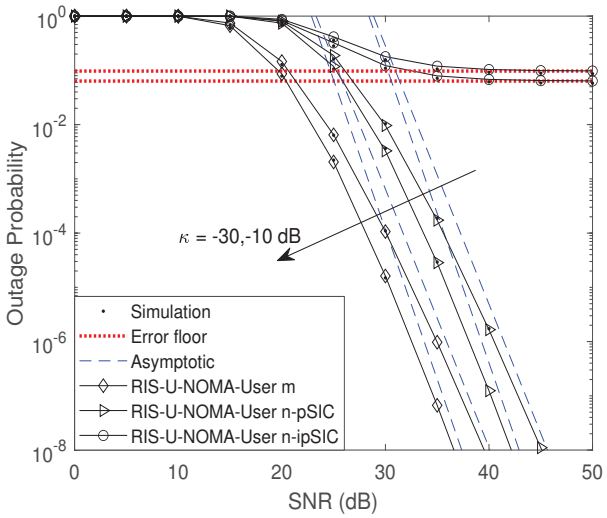

Fig. 5: Outage probability versus the transmit SNR, with $Q = 2$, $K = 50$, $\mathbb{E}\{\|\mathbf{h_I}\|^2\} = -30$ dB, $R_m = 0.5$ and $R_n = 0.5$ BPCU.

Fig. 5 plots the outage probability of RIS-U-NOMA networks versus SNR including different Rician factors, with $Q = 2$, $K = 50$ and $\mathbb{E}\{\|\mathbf{h_I}\|^2\} = -30$ dB. We can observe that the Rician factor κ has a certain influence on the performance of the RIS-U-NOMA networks. As κ grows from -30 dB to -10 dB, the outage probability of user n will decrease, thus the system performance will become better. The outage behaviors of user m will also have the same trend. This is because the LoS component dominates the Rician fading channel, which determined by Rician factor κ. As a further advance, Fig. 6 depicts the relationship between outage probability and SNR in RIS-U-NOMA networks with the setting of different path loss parameters. As the path loss exponent increases, the pass loss expression $d^{-\alpha}$ will decrease, which means the channel gain will decrease. It will cause the outage behaviors of user n and user m becomes worse. This is because the propagation environment and distance are the

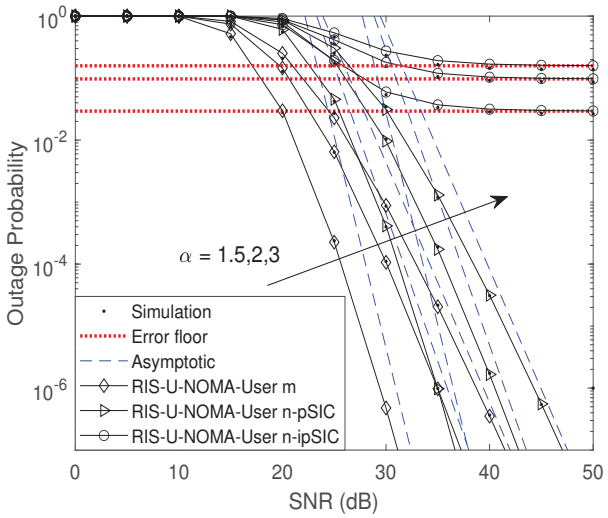

Fig. 6: Outage probability versus the transmit SNR, with $Q = 2$, $K = 50$, $\kappa = -10$ dB, $\mathbb{E}\{\|\mathbf{h_I}\|^2\} = -30$ dB, $R_m = 0.5$ and $R_n = 0.5$ BPCU.

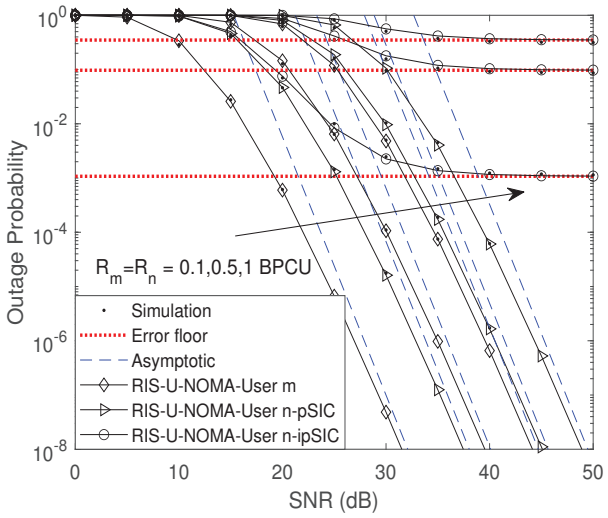

Fig. 7: Outage probability versus the transmit SNR, with $Q = 2$, $K = 50$, $\kappa = -10$ dB and $\mathbb{E}\{\|\mathbf{h_I}\|^2\} = -30$ dB.

determinants of the pass loss expression. When the path loss expression is relatively small, it indicates that the environment of the signal propagation path is poor. It can be concluded that in practical applications, RIS can be deployed flexibly to improve path quality to reduce the probability of outage events. For example, the RIS can be arranged in an open place by unmanned aerial vehicle (UAV) to obtain better channel conditions and greater Rician factors, which will be beneficial for outage performance. At the same time, according to the channel feedback, the UAV can be adjusted to be in a position with better channel conditions at all times. Moreover, Fig. 7 describes the relationship between the outage probability and SNR. The target rates are variable parameters from 0.1 to 1 BPCU, with the setting of $R_m = R_n$. It can be noted that the

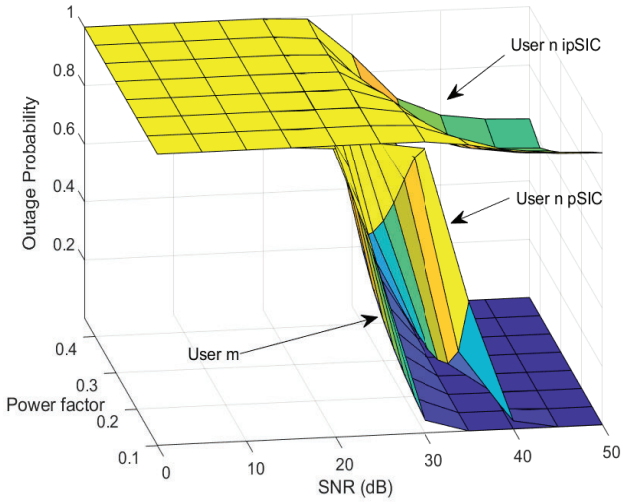

Fig. 8: Outage probability versus the transmit SNR and $\tilde{a}$, with $Q = 2$, $K = 50$, $\kappa = -10$ dB, $\mathbb{E}\{\|\mathbf{h_I}\|^2\} = -30$ dB.

outage probability of the RIS-U-NOMA networks gets larger as the target rate increases. This is due to the user's target SNR is a function of the target rate, i.e., an increase in the target rate results in larger target SNR. It is beneficial to pair users with large target rate differences, which can be favorable to the application of SIC. It is also worth noting that the parameters of small target rate can be applied to the rapidly developing Internet of Things scenarios.

Fig. 8 plots the outage probability versus SNR and the power allocation factor $\tilde{a}$, $\tilde{a} \in (0, 1)$. Other parameters are set to be $Q = 2$, $K = 50$, $\kappa = -10$ dB, $R_m = 0.5$ and $R_n = 0.5$ BPCU. Let $a_n = \tilde{a}$ and $a_m = 1 - \tilde{a}$, which also satisfies the relationship with $a_n < a_m$, i.e., $\tilde{a} < 0.5$. Based on (12) , (13) and (18), we plotted the analytical curves of outage probability of user n with ipSIC and pSIC, user m, respectively. As observed from the figure, the performance of user n with ipSIC and pSIC get better with the value of $\tilde{a}$ increases. However, the outage behavior of user m is steadily worse. The basic reason for this behavior is that the power of user m is reduced, while it suffers stronger interference signals. Therefore, it is noteworthy to optimize the power allocation factor for paired users, for the purpose of fairness and performance balance between paired users.

B. Ergodic Rate

Fig. 9 plots the ergodic rates versus SNR, with the parameters of $Q = 2$, $K = 50$, $\kappa = -10$ dB and $\mathbb{E}\{\|\mathbf{h_I}\|^2\} = -30$ dB. The ergodic rates for user n with pSIC and user m are plotted by diamond and circle solid curves according to (33) and (37), respectively. Based on (32), the pink triangle solid line is used to depict the ergodic rate of user n with the case of ipSIC, whose date is obtained by Monte Carlo simulation. Due to the influence of residual interference, that will converge to a constant value in high SNR region. As can be observed from the figure, the ergodic rate of user m also tends to a constant at high SNRs, which is higher than

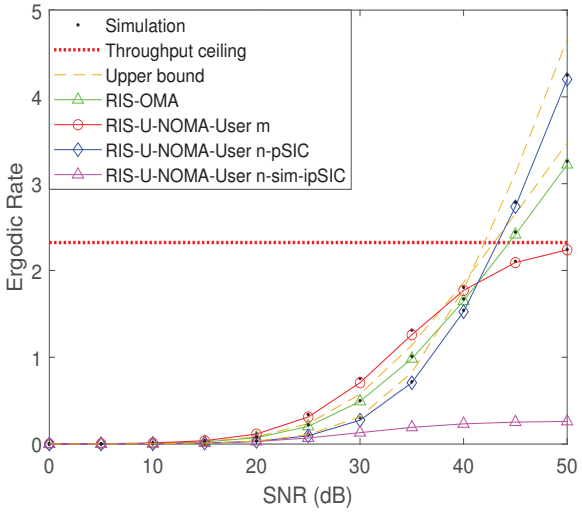

Fig. 9: Ergodic rate versus the transmit SNR, with $Q = 2$, $K = 50$, $\kappa = -10$ dB and $\mathbb{E}\{\|\mathbf{h_I}\|^2\} = -30$ dB.

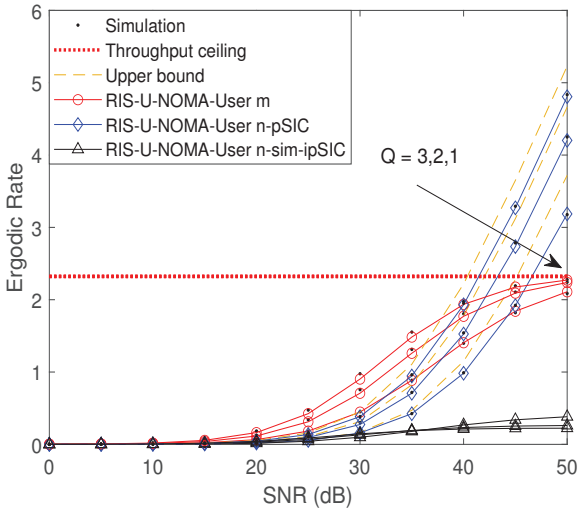

Fig. 10: Ergodic rate versus the transmit SNR, with $K = 50$, $\kappa = -10$ dB and $\mathbb{E}\{\|\mathbf{h_I}\|^2\} = -30$ dB.

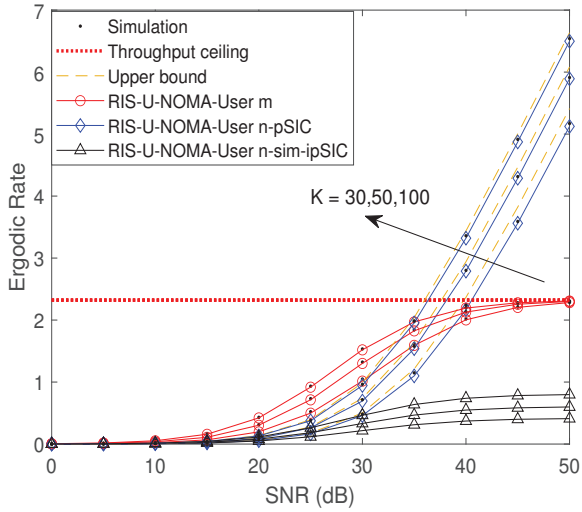

Fig. 11: Ergodic rate versus the transmit SNR, with $Q = 2$, $\kappa = -10$ dB and $\mathbb{E}\{\|\mathbf{h_I}\|^2\} = -30$ dB.

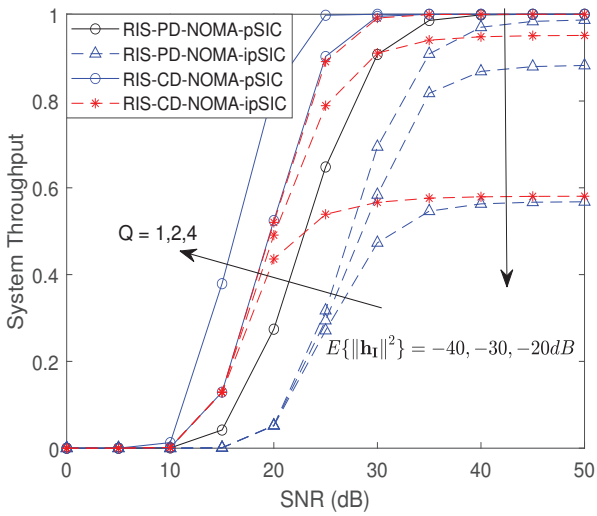

Fig. 12: System throughput in delay-limited transmission mode versus SNR, with $\kappa = -10$ dB, $\alpha = 2$ and $K = 50$.

that in ipSIC case. This constant is represented as throughput ceiling and plotted by the red dotted line, which means a zero high SNR slope. This is consistent with the conclusion in the **Remark 5**. In addition, khaki dotted line is picked to plot the upper bound curve for ergodic rate, which gives a better approximation. An important observation can be seen from Fig. 9 that in the high SNR regime, the ergodic rate of user n with pSIC outperforms than that of OMA users. However, the ergodic rate of user m is inferior to OMA. This is because the high SNR slopes of the above three satisfy the relationship of $S_{n,pSIC} > S_{OMA} > S_m$, which can be obtained from **Remark 4**, **Remark 5** and **Remark 6**. To illustrate the impact of subcarrier numbers on ergodic rates, Fig. 10 plots the ergodic rates versus SNR with different values of Q. With the decrease of Q, the ergodic rates of user m and n decrease significantly. Moreover, the ergodic rates of user m with different Q eventually converge to a same throughput ceiling, which is consistent with the discussion in **Remark 5**. From this discovery, we can achieve the same rate at high SNRs through reasonable user pairing with fewer subcarriers Q. In order to obtain more comprehensive analytical results, Fig. 11 plots the ergodic rates versus SNR with different reconfigurable elements. As the number of K grows, user n and m are capable of obtaining larger ergodic rates. Additionally, the growth rate of user n with pSIC is larger than other cases, which is associated with high SNR slope.

C. System Throughput

Fig. 12 plots the system throughput versus transmit SNR for RIS-U-NOMA networks in delay-limited transmission mode. According to (46), we obtain the system throughput curves with ipSIC/pSIC. In the case of pSIC, the blue and black solid lines represent the throughput in RIS-CD-NOMA and RIS-PD-NOMA, respectively. As the number of subcarriers increases, the RIS-U-NOMA networks can provide enhanced system throughput. It is worth noting that at high SNRs, different Q will achieve the same throughput. This can be explained by the fact that both user n and user m can achieve lower outage probability, which has little impact on the system throughput. As for the case of ipSIC, the system throughput with $Q = 2$ and $Q = 1$ are represented by the red and blue dashed lines, respectively. We observe the case of $Q = 2$ achieves higher throughput compared to $Q = 1$, which means RIS-CD-NOMA can achieve better throughput than RIS-PD-NOMA. Meanwhile, with the residual interference increasing from -40dB to -20dB, the system throughput will descend. It can be found when $\mathbb{E}\{\|\mathbf{h_I}\|^2\} = -40dB$, the system throughput is very close to the throughput of pSIC. This is because the effect of residual interference is small compared to the user signals. Another finding is that with the value of residual interference increasing from -40 dB to -20 dB, the system throughput with same Q does not change much at low SNRs. However, there is a significant decrease in the high SNR region due to the error floor. Therefore, the impact of ipSIC on system performance needs to be considered in practical networks.

VI. Conclusion

In this paper, the RIS-U-NOMA framework is proposed, where the performance of the RIS-U-NOMA framework is characterized by outage probability, ergodic rate and system throughput. We have derived the new approximated expressions of the outage probability for user n with ipSIC/pSIC and user m. According to the asymptotic expressions in high SNR regime, the diversity order are attained carefully. The results specified that the outage behavior of RIS-U-NOMA is better than that of RIS-OMA and conventional FD/HD-DF relays. Except for ipSIC case, the diversity order of RIS-CD-NOMA is Q times that of RIS-PD-NOMA. In addition, the ergodic rate of user n and m and their corresponding high SNR slope have been derived. According to the analysis results, it has been demonstrated that the ergodic rate of RIS-CD-NOMA outperforms that of RIS-PD-NOMA. Finally, the system throughput in delay-limited and delay-tolerant modes has been studied. Numerical results verified the outcome of the analysis. Based on the multiple scenarios and limited physical resources, flexible switching of the mode in RIS-U-NOMA framework is a promising future research direction.

Appendix A: Proof of Theorem 1

The proof process starts by substituting (5) and (6) into (11). Without loss of generality, we suppose $\mathbf{g}_m$ and $\mathbf{g}_n$ have the same weight in each column in $\mathbf{G}_{Q\times M}$, which means $\left\|diag(\mathbf{h}_n + \widetilde{\mathbf{h}}_{Rn}^H \mathbf{\Theta}_n \widetilde{\mathbf{h}}_{br})\mathbf{g}_n\right\|^2$ and $\left\|diag(\mathbf{h}_m + \widetilde{\mathbf{h}}_{Rm}^H \mathbf{\Theta}_m \widetilde{\mathbf{h}}_{br})\mathbf{g}_m\right\|^2$ own the same distribution. By applying the coherent phase shifting and some standard mathematical manipulation, the expression of outage probability of user n with ipSIC can be obtained as

$$P_{n,ipSIC}^{RIS-CD} = \Pr\left[\underbrace{\left\|diag(\mathbf{h}_n + \widetilde{\mathbf{h}}_{Rn}^H \mathbf{\Theta}_n \widetilde{\mathbf{h}}_{br})\mathbf{g}_n\right\|^2}_{Z_n} < \xi\left(\psi|h_I|^2\rho + 1\right)\right], \tag{A.1}$$

where $\psi = 1$, $\xi \triangleq \max(\tau, \beta)$, $\tau = \frac{\varepsilon_m}{\rho(a_m - \varepsilon_m a_n)}$ and $\beta = \frac{\varepsilon_n}{\rho a_n}$.

It is necessary to obtain the CDF of variable Z_n to complete the proof process and we will derive it below. It can be observed that

$$Z_n = \sum_{i=1}^{Q}\left|h_{ni} + \sum_{k=1}^{K}\left|\widetilde{h}_{Rnik}\widetilde{h}_{bri}\right|\right|^2 \tag{A.2}$$

and it is difficult to directly solve the CDF and PDF of it. Let $z_i = \left|h_{ni} + \sum_{k=1}^{K}\left|\widetilde{h}_{Rnik}\widetilde{h}_{bri}\right|\right|$ and we can get a simplified expression $Z_n = \sum_{i=1}^{Q} z_i^2$. With the aid of Jensen Inequality, the expression of Z_n can be given by

$$Z_n \geq \frac{1}{Q}\left(\sum_{i=1}^{Q} z_i\right)^2 = T_n. \tag{A.3}$$

When $z_1 = \cdots = z_Q$, the equality of inequalities is obtained. Substituting (A.3) into (A.1), an approximated expression of the outage probability for user n can be expressed as

$$P_n \approx \Pr\left[\widetilde{T_n} = \sum_{i=1}^{Q} z_i < \sqrt{Q\xi\left(\psi|h_I|^2\rho + 1\right)}\right]. \tag{A.4}$$

So far, the issue of solving Z_n has been transformed into the CDF problem of $\widetilde{T_n}$. Based on the two characteristic features of cascade Rician fading channels [47], i.e., 1) the maximum value of the PDF is unique; 2) the PDF curve can extend infinitely on both sides of the maximum value. Hence, we can approximate this type of PDF expression by applying a series of Laguerre polynomials. With the help of [47, Eq. (2.76)], the PDF of $\widetilde{T_n}$ can be approximated as

$$f_{\widetilde{T_n}}(t) \approx \frac{t^{\varphi_z}}{\phi_n^{\varphi_z+1}\Gamma(\varphi_z+1)}\exp\left(-\frac{t}{\phi_z}\right), \tag{A.5}$$

where $\varphi_z = \frac{\mu_z^2 Q}{\sigma_z^2} - 1$ and $\phi_z = \frac{\sigma_z^2}{\mu_z}$. μ_z and σ_z^2 are the mean and variance of z_i, respectively. Let $y_i = \sum_{k=1}^{K}\left|\widetilde{h}_{Rnik}\widetilde{h}_{bri}\right|$ and $z_i = |x_i + y_i|$. On the basis of [48], we can get the expression of the mean and variance of y_i as

$$\mu_{y_i} = \tau_b\frac{\Gamma(\tau_a+2)}{\Gamma(\tau_a+1)}, \tag{A.6}$$

and

$$\sigma_{y_i}^2 = \frac{\tau_b^2\left[\Gamma(\tau_a+3)\Gamma(\tau_a+1) - (\Gamma(\tau_a+2))^2\right]}{[\Gamma(\tau_a+1)]^2}, \tag{A.7}$$

where $\tau_a = \frac{\mu_{cc}^2 K}{\sigma_{cc}^2} - 1$ and $\tau_b = \frac{\sigma_{cc}^2}{\mu_{cc}}$. μ_{cc} and σ_{cc}^2 can be obtained from (9) and (10). As a further advance, the CDF of $\widetilde{T_n}$ can be given by

$$F_{\widetilde{T_n}}(t) = \int_0^t \frac{t^{\varphi_z}}{{\phi_n}^{\varphi_z+1}\Gamma(\varphi_z+1)} \exp\left(-\frac{t}{\phi_z}\right) dt = \left[\Gamma(\varphi_z+1)\right]^{-1} \gamma\left(\varphi_z+1, \frac{t}{\phi_z}\right). \quad \text{(A.8)}$$

In addition, the PDF of residual interference can be written as

$$f_{|h_I|^2}(y) = \frac{y^{Q-1} e^{-\frac{y}{\Omega_I}}}{(Q-1)!\Omega_I^Q}. \quad \text{(A.9)}$$

After some manipulations, the outage probability of user n with ipSIC can be further calculated as

$$P_{n,ipSIC}^{RIS-CD} = \int_0^\infty \frac{y^{Q-1} e^{-\frac{y}{\Omega_I}}}{(Q-1)!\Omega_I^Q} \left[\Gamma(\varphi_z+1)\right]^{-1} \times \gamma\left(\varphi_z+1, \frac{\sqrt{Q\xi(\psi y\rho+1)}}{\phi_z}\right) dy. \quad \text{(A.10)}$$

As a further development, the above indefinite integral [49, Eq. (8.6.5)] can be approximated by Gauss-Laguerre quadrature, which is given by

$$\int_0^\infty f(x) e^{-x} dx \approx \sum_{u=1}^{U} H_u f(x_u). \quad \text{(A.11)}$$

Utilize (A.11) into (A.10) to obtain (12). The proof is completed.

Appendix B: Proof of Theorem 2

Upon substituting (6) into (17), the outage probability of user m can be given by

$$P_m^{RIS-CD} = \Pr\left[\underbrace{\left\|diag(\mathbf{h}_m + \widetilde{\mathbf{h}}_{Rm}^H \mathbf{\Theta}_m \widetilde{\mathbf{h}}_{br})\mathbf{g}_m\right\|^2}_{Z_m} < \frac{\varepsilon_m}{\rho(a_m - \varepsilon_m a_n)}\right], \quad \text{(B.1)}$$

where ε_m is the target SNR with the relationship $a_m > \varepsilon_m a_n$. From the derived process in Appendix A, the CDF of Z_m can be written as

$$F_{Z_m}(z) \approx \left[\Gamma(\varphi_z+1)\right]^{-1} \gamma\left(\varphi_z+1, \frac{\sqrt{Qz}}{\phi_z}\right), \quad \text{(B.2)}$$

Substitute (B.2) into (B.1) and perform some math substitutions to obtain (18). The proof is completed.

Appendix C: Proof of Theorem 5

Based on (6), the ergodic rate of user m in RIS-U-NOMA networks can be calculated as (C.1) at the top of next page.

Via the assistance of (18) and coherent phase shifting, the CDF of J can be represented as

$$F_J(x) = \gamma\left(\varphi_J+1, (\phi_J)^{-1}\sqrt{Q\left(\frac{x}{\rho(a_m - x a_n)}\right)}\right) \times \left[\Gamma(\varphi_J+1)\right]^{-1} \quad \text{(C.2)}$$

where $a_m > x a_n$. Substituting (C.2) into (C.1), the ergodic rate of user m can be expressed as (37). The proof is completed.

References

[1] K. B. Letaief, W. Chen, Y. Shi, J. Zhang, and Y.-J. A. Zhang, "The roadmap to 6G: AI empowered wireless networks," *IEEE Commun. Mag.*, vol. 57, no. 8, pp. 84–90, 2019.
[2] W. U. Khan, J. Liu, F. Jameel, V. Sharma, R. Jäntti, and Z. Han, "Spectral efficiency optimization for next generation NOMA-enabled IoT networks," *IEEE Trans. Veh. Technol.*, vol. 69, no. 12, pp. 15 284–15 297, 2020.
[3] Y. Yuan, S. Wang, Y. Wu, H. V. Poor, Z. Ding, X. You, and L. Hanzo, "NOMA for next-generation massive IoT: Performance potential and technology directions," *IEEE Commun. Mag.*, vol. 59, no. 7, pp. 115–121, 2021.
[4] Y. Liu, W. Yi, Z. Ding, X. Liu, O. Dobre, and N. Al-Dhahir, "Application of NOMA in 6G networks: Future vision and research opportunities for next generation multiple access," 2021. [Online]. Available: https://arxiv.org/abs/2103.02334v1.
[5] D. Tse and P. Viswanath, *Fundamentals of wireless communication*, Cambridge University Press, Cambridge, UK, 2005.
[6] Z. Ding, Y. Liu, J. Choi, Q. Sun, M. Elkashlan, I. Chih-Lin, and H. V. Poor, "Application of non-orthogonal multiple access in LTE and 5G networks," *IEEE Commun. Mag.*, vol. 55, no. 2, pp. 185–191, 2017.
[7] X. Yue, Z. Qin, Y. Liu, S. Kang, and Y. Chen, "A unified framework for non-orthogonal multiple access," *IEEE Trans. Commun.*, vol. 66, no. 11, pp. 5346–5359, 2018.
[8] Z. Qin, X. Yue, Y. Liu, Z. Ding, and A. Nallanathan, "User association and resource allocation in unified NOMA enabled heterogeneous ultra dense networks," *IEEE Commun. Mag.*, vol. 56, no. 6, pp. 86–92, 2018.
[9] Z. Ding, X. Lei, G. K. Karagiannidis, R. Schober, J. Yuan, and V. K. Bhargava, "A survey on non-orthogonal multiple access for 5G networks: Research challenges and future trends," *IEEE J. Sel. Areas Commun.*, vol. 35, no. 10, pp. 2181–2195, 2017.
[10] L. Dai, B. Wang, Z. Ding, Z. Wang, S. Chen, and L. Hanzo, "A survey of non-orthogonal multiple access for 5G," *IEEE Commun. Surv. Tuts.*, vol. 20, no. 3, pp. 2294–2323, 2018.
[11] Z. Ding, Z. Yang, P. Fan, and H. V. Poor, "On the performance of non-orthogonal multiple access in 5G systems with randomly deployed users," *IEEE Signal Process. Lett.*, vol. 21, no. 12, pp. 1501–1505, 2014.
[12] O. Maraqa, A. S. Rajasekaran, S. Al-Ahmadi, H. Yanikomeroglu, and S. M. Sait, "A survey of rate-optimal power domain NOMA with enabling technologies of future wireless networks," *IEEE Commun. Surv. Tuts.*, vol. 22, no. 4, pp. 2192–2235, 2020.
[13] M. Amjad and L. Musavian, "Performance analysis of NOMA for ultra-reliable and low-latency communications," in *IEEE Proc. of Globecom Workshops (GC Wkshps)*, 2018, pp. 1–5.
[14] L. Yu, P. Fan, X. Lei, and P. T. Mathiopoulos, "BER analysis of SCMA systems with codebooks based on Star-QAM signaling constellations," *IEEE Commun. Lett.*, vol. 21, no. 9, pp. 1925–1928, 2017.
[15] X. Dai, Z. Zhang, B. Bai, S. Chen, and S. Sun, "Pattern division multiple access: A new multiple access technology for 5G," *IEEE Wireless Commun.*, vol. 25, no. 2, pp. 54–60, 2018.
[16] W. Tang, S. Kang, and B. Ren, "Performance analysis of cooperative pattern division multiple access (Co-PDMA) in uplink network," *IEEE Access*, vol. 5, pp. 3860–3868, 2017.
[17] X. Dai, T. Yan, Q. Li, H. Li, and X. Wang, "Pattern division random access (PDRA) for M2M communications with massive MIMO systems," *IEEE Trans. Veh. Technol.*, vol. 70, no. 12, pp. 12 631–12 639, 2021.
[18] Y. Liu, S. Zhang, X. Mu, Z. Ding, R. Schober, N. Al-Dhahir, E. Hossain, and X. Shen, "Evolution of NOMA toward next generation multiple access (NGMA) for 6G," 2021. [Online]. Available: https://arxiv.org/abs/2108.04561
[19] Y. Liu, W. Yi, Z. Ding, X. Liu, O. Dobre, and N. Al-Dhahir, "Developing NOMA to next generation multiple access (NGMA): Future vision and research opportunities," 2021. [Online]. Available: https://arxiv.org/abs/2103.02334
[20] X. Yu, D. Xu, Y. Sun, D. W. K. Ng, and R. Schober, "Robust and secure wireless communications via intelligent reflecting surfaces," *IEEE J. Sel. Areas Commun.*, vol. 38, no. 11, pp. 2637–2652, 2020.
[21] Q. Wu and R. Zhang, "Towards smart and reconfigurable environment: Intelligent reflecting surface aided wireless network," *IEEE Commun. Mag.*, vol. 58, no. 1, pp. 106–112, 2020.

$$R_m^{erg} = \mathbb{E}\left[\log\left(1+\frac{\rho\left\|diag(\mathbf{h}_m+\widetilde{\mathbf{h}}_{Rm}^H\mathbf{\Theta}_m\widetilde{\mathbf{h}}_{br})\mathbf{g}_m\right\|^2 a_m}{\underbrace{\rho\left\|diag(\mathbf{h}_m+\widetilde{\mathbf{h}}_{Rm}^H\mathbf{\Theta}_m\widetilde{\mathbf{h}}_{br})\mathbf{g}_n\right\|^2 a_n+1}_{J}}\right)\right] = \frac{1}{\ln 2}\int_0^\infty \frac{1-F_J(x)}{1+x}dx \tag{C.1}$$

[22] S. Basharat, S. A. Hassan, H. Pervaiz, A. Mahmood, Z. Ding, and M. Gidlund, "Reconfigurable intelligent surfaces: Potentials, applications, and challenges for 6G wireless networks," *IEEE Wirel. Commun.*, vol. 28, no. 6, pp. 184–191, 2021.

[23] M. A. ElMossallamy, H. Zhang, L. Song, K. G. Seddik, Z. Han, and G. Y. Li, "Reconfigurable intelligent surfaces for wireless communications: Principles, challenges, and opportunities," *IEEE Trans. Cogn. Commun. Netw.*, vol. 6, no. 3, pp. 990–1002, 2020.

[24] C. Huang, A. Zappone, G. C. Alexandropoulos, M. Debbah, and C. Yuen, "Reconfigurable intelligent surfaces for energy efficiency in wireless communication," *IEEE Trans. Wireless Commun.*, vol. 18, no. 8, pp. 4157–4170, 2019.

[25] H. Guo, Y.-C. Liang, J. Chen, and E. G. Larsson, "Weighted sum-rate maximization for reconfigurable intelligent surface aided wireless networks," *IEEE Trans. Wireless Commun.*, vol. 19, no. 5, pp. 3064–3076, 2020.

[26] H. Shen, W. Xu, S. Gong, Z. He, and C. Zhao, "Secrecy rate maximization for intelligent reflecting surface assisted multi-antenna communications," *IEEE Commun. Lett.*, vol. 23, no. 9, pp. 1488–1492, 2019.

[27] T. Hou, Y. Liu, Z. Song, X. Sun, Y. Chen, and L. Hanzo, "Reconfigurable intelligent surface aided NOMA networks," *IEEE J. Sel. Areas Commun.*, vol. 38, no. 11, pp. 2575–2588, 2020.

[28] Y. Cheng, K. H. Li, Y. Liu, K. C. Teh, and H. Vincent Poor, "Downlink and uplink intelligent reflecting surface aided networks: NOMA and OMA," *IEEE Trans. Wireless Commun.*, vol. 20, no. 6, pp. 3988–4000, 2021.

[29] G. Yang, X. Xu, Y.-C. Liang, and M. D. Renzo, "Reconfigurable intelligent surface-assisted non-orthogonal multiple access," *IEEE Trans. Wireless Commun.*, vol. 20, no. 5, pp. 3137–3151, 2021.

[30] Z. Zhang, J. Chen, Y. Liu, Q. Wu, B. He, and L. Yang, "On the secrecy design of STAR-RIS assisted uplink NOMA networks," *IEEE Trans. Wireless Commun.*, pp. 1–1, 2022.

[31] V. C. Thirumavalavan and T. S. Jayaraman, "BER analysis of reconfigurable intelligent surface assisted downlink power domain NOMA system," in *IEEE Proc. of Int. Conf. COMmun. Syst. NETworkS (COMSNETS)*, 2020, pp. 519–522.

[32] Z. Ding and H. Vincent Poor, "A simple design of IRS-NOMA transmission," *IEEE Commun. Lett.*, vol. 24, no. 5, pp. 1119–1123, 2020.

[33] Z. Ding, R. Schober, and H. V. Poor, "On the impact of phase shifting designs on IRS-NOMA," *IEEE Wireless Commun. Lett.*, vol. 9, no. 10, pp. 1596–1600, 2020.

[34] X. Liu, Y. Liu, Y. Chen, and H. V. Poor, "RIS enhanced massive non-orthogonal multiple access networks: Deployment and passive beamforming design," *IEEE J. Sel. Areas Commun.*, vol. 39, no. 4, pp. 1057–1071, 2021.

[35] S. Sharma, K. Deka, Y. Hong, and D. Dixit, "Intelligent reflecting surface-assisted uplink SCMA system," *IEEE Commun. Lett.*, vol. 25, no. 8, pp. 2728–2732, 2021.

[36] I. Al-Nahhal, O. A. Dobre, and E. Basar, "Reconfigurable intelligent surface-assisted uplink sparse code multiple access," *IEEE Commun. Lett.*, vol. 25, no. 6, pp. 2058–2062, 2021.

[37] A. Bansal, K. Singh, B. Clerckx, C.-P. Li, and M.-S. Alouini, "Rate-splitting multiple access for intelligent reflecting surface aided multi-user communications," *IEEE Trans. Veh. Technol.*, vol. 70, no. 9, pp. 9217–9229, 2021.

[38] X. Yue and Y. Liu, "Performance analysis of intelligent reflecting surface assisted NOMA networks," *IEEE Trans. Wireless Commun.*, vol. 21, no. 4, pp. 2623–2636, 2022.

[39] Y. Chen, A. Bayesteh, Y. Wu, B. Ren, S. Kang, S. Sun, Q. Xiong, C. Qian, B. Yu, Z. Ding, S. Wang, S. Han, X. Hou, H. Lin, R. Visoz, and R. Razavi, "Toward the standardization of non-orthogonal multiple access for next generation wireless networks," *IEEE Commun. Mag.*, vol. 56, no. 3, pp. 19–27, 2018.

[40] W. Tang, M. Z. Chen, X. Chen, J. Y. Dai, Y. Han, M. Di Renzo, Y. Zeng, S. Jin, Q. Cheng, and T. J. Cui, "Wireless communications with reconfigurable intelligent surface: Path loss modeling and experimental measurement," *IEEE Trans. Wireless Commun.*, vol. 20, no. 1, pp. 421–439, 2021.

[41] J. Choi, "On the power allocation for a practical multiuser superposition scheme in NOMA systems," *IEEE Commun. Lett.*, vol. 20, no. 3, pp. 438–441, Mar. 2016.

[42] Y. Sun, D. W. K. Ng, Z. Ding, and R. Schober, "Optimal joint power and subcarrier allocation for full-duplex multicarrier non-orthogonal multiple access systems," *IEEE Trans. Commun.*, vol. 65, no. 3, pp. 1077–1091, 2017.

[43] M. K. Simon, *Probability Distributions Involving Gaussian Random Variables*. Springer US, 2006.

[44] X. Yue, J. Xie, Y. Liu, Z. Han, R. Liu, and Z. Ding, "Simultaneously transmitting and reflecting reconfigurable intelligent surface assisted NOMA networks." [Online]. Available: https://arxiv.org/abs/2112.01336v3.

[45] I. S. Gradshteyn and I. M. Ryzhik, *Table of Integrals, Series and Products*, 6th ed. New York, NY, USA: Academic Press, 2000.

[46] C. Zhang, W. Yi, Y. Liu, Z. Ding, and L. Song, "STAR-IOS aided NOMA networks: Channel model approximation and performance." [Online]. Available: https://arxiv.org/abs/2107.01543v1.

[47] Primak, S. Kontorovitch, V. Lyandres, and Vladimir, *Stochastic Methods and their Applications to Communications: Stochastic Differential Equations Approach*, West Sussex, U.K.: Wiley, 2004.

[48] A. M. Salhab and M. H. Samuh, "Accurate performance analysis of reconfigurable intelligent surfaces over rician fading channels," *IEEE Wireless Commun. Lett.*, vol. 10, no. 5, pp. 1051–1055, 2021.

[49] E. Hildebrand, *Introduction to numerical analysis*, New York, NY, USA: Dover, 1987.